Holness, M. B., Gautier, N., Rust, A. C., & Neufeld, J. (2022). The Microstructural Record of Convection in the Little Minch Sill Complex, Scotland. *Journal of Petrology*, *63*(11), [egac106]. https://doi.org/10.1093/petrology/egac106

University of Bristol - Explore Bristol Research
General rights

OXFORD

The Microstructural Record of Convection in the Little Minch Sill Complex, Scotland

Marian B. Holness [ID][1,*], Gautier Nicoli[2], Alison Rust[3] and Jerome Neufeld[1,4,5]

[1]Department of Earth Sciences, University of Cambridge, Downing Street, Cambridge CB2 3EQ, UK
[2]Institut für Geowissenschaften, Universität Potsdam, 14476 Potsdam-Golm, Germany
[3]School of Earth Sciences, University of Bristol, Wills Memorial Building, Queens Road, Clifton, Bristol BS8 1RJ, UK
[4] BP Institute for Multiphase Flow, University of Cambridge, Madingley Road, Cambridge CB3 0EZ, UK
[5]Department of Applied Mathematics and Theoretical Physics, University of Cambridge, Centre for Mathematical Sciences, Wilberforce Road, Cambridge CB3 0WA, UK

*Corresponding author. E-mail: marian@esc.cam.ac.uk

Abstract

Detailed microstructural analysis of three basaltic sills of the Little Minch Sill Complex demonstrates that convection leaves a detectable signature in fully solidified bodies. The presence of dense clusters of equant grains of olivine and clinopyroxene in the central parts of sills can only be accounted for if they formed and were enlarged while suspended in convecting magma, with delayed settling to the sill floor. An associated stratigraphic invariance of plagioclase grain shape is consistent with growth while suspended in convecting magma. These microstructural indicators demonstrate that convection during solidification was vigorous and long-lived in the 135-m-thick picrodolerite-crinanite unit (PCU) of the composite Shiant Isles Main sill and vigorous and likely short-lived in the PCU of the composite Creagan Iar sill. In contrast, convection in the Meall Tuath sill was weak and short-lived: plagioclase grain shape in this sill varies with stratigraphic height, indicative of primarily *in situ* nucleation and growth at the magma-mush interface, while olivine and clinopyroxene were kept suspended in the overlying convecting magma. The magma in all three sills fractionated during solidification, permitting convection driven by the instability of an upper thermal boundary layer. The comparative vigour and longevity of convection in the Shiant Isles Main sill and the Creagan Iar sill was due to their emplacement above an earlier, still-hot, intrusion, resulting in highly asymmetric cooling.

INTRODUCTION

The fundamental link between magma fluid dynamical behaviour and its chemical evolution necessitates constraining the extent to which magmas convect during solidification, although early attempts to solve this problem proved contentious (Marsh, 1989, 1991; Sparks, 1990; Huppert & Turner, 1991; Gibb & Henderson, 1992). While some authors advocate a short and transient period of thermally driven convection (Brandeis & Marsh, 1989, 1990; Marsh, 1989, 1991; Bea, 2010), others argue for sustained and continuous convection during most of the solidification history, driven by thermal or compositional gradients (Worster et al., 1990; Huppert & Turner, 1991), or by the descent of dense, crystal-bearing, material from the roof (Bergantz & Ni, 1999; Philpotts & Dickson, 2000; Philpotts & Philpotts, 2005).

Much of the earlier work is reliant on conclusions based variously on assumed values of temperature differences driving convective flow (Marsh, 1991), analytical models (e.g. Worster et al., 1990) or observations of low-temperature analogues (e.g. Brandeis & Marsh, 1989, 1990). In this contribution, we build on the work of Holness et al. (2017a) and Dyck & Holness (2021), who argued that the presence, and stratigraphic variation in size, of crystal clusters in fully solidified magma bodies provides evidence of vigorous long-lived convection. We report the results of a detailed microstructural examination of mafic sills belonging to the Little

Minch Sill Complex and argue that the stratigraphic variation of plagioclase grain shape may also record convection and that vigorous and long-lived convection may be common in composite sills.

PREVIOUS WORK
Convection and crystal settling in sills

A horizontal tabular body of basaltic magma intruded into the crust will conduct heat into the cooler material above and below, generating density gradients that may drive thermal convection of the magma. Density changes resulting from changes in liquid composition due to crystallisation may also drive compositional convection.

Compositional convection is caused by the creation of a buoyant residual melt by crystallisation at the floor or a dense residual melt created at the roof—the former is most common in basaltic systems (e.g. Jaupart & Tait, 1995). Compositional convection may occur within the marginal crystal mushes or be driven by the instability of a compositional boundary layer immediately adjacent to the marginal mush zones. Whether or not convection initiates, and the vigour of the resulting convective flow, depend on a non-dimensional Rayleigh number. Convection occurs for *Ra* greater than some critical value, and the flow is more vigorous

and complex as *Ra* increases. The Rayleigh number for convection of interstitial melt in the mush, Ra_{mush}, is

$$Ra_{\mathrm{mush}} = \frac{g \Delta\rho \; k \; h}{\kappa \; \mu},$$

where $\Delta\rho$ is the difference in density across the mush layer of thickness h, g is gravitational acceleration, and κ and μ are the thermal diffusivity and viscosity of the fluid, respectively. The mush permeability, k, for crystals $\sim$1 mm in diameter and crystal volume fractions of 0.8, 0.6 and 0.4 is of order 10^{-10}, 10^{-9} and 10^{-8} m^2, respectively (Hersum et al., 2005). For these values of permeability, Rayleigh numbers only exceed the critical value of $\sim$25 required for convection if the mush thickness exceeds several hundreds of metres (Tait & Jaupart, 1992). The mush thickness in the sills discussed in this contribution was less than 10 m (see later), so compositional convection in the mush was not possible.

The Rayleigh number associated with convection driven by a chemical boundary layer of buoyant residual liquid immediately overlying the floor mush is

$$Ra_{\mathrm{compositional\ layer}} = \frac{g \Delta\rho \; \delta^3}{D \; \mu},$$

where δ is the thickness of the buoyant layer above the floor mush, $\Delta\rho$ is the difference in density across the boundary layer, and D is the diffusivity of relevant chemical species in the melt (e.g. $\sim$10^{-12} m^{2}s^{-1} for Mg^{2+} and Fe^{2+}). The thickness of the chemical boundary layer is proportional to the mush thickness until convection initiates, so the critical Ra (which is in the range 1–8; Tait & Jaupart, 1989) can also be expressed in terms of the mush thickness required to initiate convection. Using values typical of basaltic systems, Tait & Jaupart (1989) argue that the crystallisation front has to attain a thickness of $\sim$90 m before convection begins; convection driven by a compositional boundary layer is not possible in sills of order 10's of metres thickness.

Convection in basaltic sills will therefore be predominantly thermal, driven by the instability of an upper thermal boundary layer since the cool liquid in the lower thermal boundary layer will be gravitationally stable. The Rayleigh number for thermally driven convection can be expressed as

$$Ra = \frac{g \; \alpha \Delta T \; \rho \; d^3}{\kappa \; \mu},$$

where ΔT is the temperature difference across a fluid layer of thickness d and α and ρ are the thermal expansion coefficient and density of the fluid, respectively (other symbols as before). The critical value of Ra is of order 10^3. The cubic dependence of *Ra* on the length-scale d and the limited ranges of the other parameters in basaltic magma, make d the most critical parameter. The relevant value of d for the initiation of convection is the thickness of the thermal boundary layer at the magma-mush interface at the sill roof (Marsh, 1989; Jaupart & Tait, 1995). The temperature difference, or supercooling, is likely to be that required to drive nucleation and crystal growth at the upper margin of the intrusion (termed kinetic undercooling by Worster et al., 1990). Since almost all mafic bodies preserve phenocrysts in their chilled margins, and were thus saturated in at least one mineral phase on intrusion, the magnitude of the temperature difference available to drive convection immediately following intrusion is likely to be only a few degrees Celsius. For $\Delta T = 1°C$, $\mu = 10$ Pas, $\alpha = 5\times10^{-5}$, $\rho = 2750$ kg/m^3, and $\kappa = 10^{-6}$ m^2/s, *Ra* of order 10^3 is achieved for $d = 0.2$ m.

In non-fractionating bodies, the composition of the remaining bulk liquid, and hence the liquidus temperature, remain constant; thus, for simple, non-composite intrusions, once the entire magma body has cooled to the temperature at which crystals can nucleate, convection will cease. In contrast, the continuously decreasing liquidus temperature of the remaining bulk magma in a fractionating system may preserve the temperature difference between the magma and the crystallised solidification front required for thermally driven convection. The longevity of thermally driven convection is therefore fundamentally linked to fractionation (Marsh, 1989, 1991).

Destabilisation of the boundary layer results in downwelling plumes that carry suspended crystals. These plumes move through the full depth of the remaining bulk magma, and so the dynamics of convection also reflect a larger *Ra* characterised by the length scale of the full fluid depth (Huppert & Turner, 1991). Once thermal convection is initiated by destabilisation of the upper thermal boundary layer, convection in sills of order 10 m thick (i.e. $d = 10$ m) should be vigorous. However, *Ra* will decrease with time, both because d decreases with progressive solidification and because of increasing viscosity (μ) of the cooling and evolving magma.

Although sinking magma can carry crystals downwards, upwellings can only entrain crystals (and crystal clusters) if flow exceeds their fall velocity, which is dependent on crystal (or cluster) size. Particles with terminal velocities much lower than mean flow velocity can remain in suspension for extended times (e.g. Patočka et al., 2022), eventually accumulating on the floor (or getting trapped in the downwards-migrating roof sequence) when the convective flow brings them into the marginal boundary layers in which flow velocities are vanishingly small (e.g. Martin & Nokes, 1989). If magma plumes sinking from the roof remain sufficiently cool and dense, they pool at the floor, creating a progressively thicker basal layer of cool, stable magma with convective flow continuing only in the magma above it. This is a form of 'filling box' convection (Turner, 1979) and facilitates crystal accumulation at the floor. However, cooling through the base will be reduced if the sill is emplaced over a warm (e.g. partially molten) layer, such as might occur in a composite body. This will slow down the overall cooling rate, thus maintaining higher *Ra* for longer, and so enabling convection initiated at the top of the sill to occur more readily and to be more vigorous than for the same sill with cold country rock at its base.

Microstructural evidence for convection preserved in fully solidified intrusions

Evidence of fractionation in sills, and hence the *possibility* of long-lived convection, is provided by the position of the sandwich horizon—that stratigraphic position where the roof and floor solidification fronts meet. This is usually the position of the most evolved composition (neglecting the possibility of localised segregation of late-stage evolved liquids into tears in the upper solidification front as described by Marsh, 1996). The sandwich horizon occurs significantly above the stratigraphic mid-point in systems in which the solids were predominantly denser than the residual liquid and ended up on the floor. However, an unambiguous indicator of convection during solidification can be provided by a detailed analysis of grain size and clustering in the particle accumulations at floor and roof.

Because the presence of a crystal cargo in the incoming magma can delay the onset of convection (Koyaguchi et al., 1990), immediately following intrusion a crystal-rich magma may be static

until settling reduces the particle concentration, creating a fining-upwards floor sequence typified by coarse-tail grading, and a fining-downwards sequence at the roof (e.g. Marsh, 1988). The onset of convection changes both the rate of settling (e.g. Marsh & Maxey, 1985; Martin & Nokes, 1988) and the grain size profile of the crystal accumulations at the floor and roof (e.g. Jarvis & Woods, 1994). Although a fining-upwards accumulation is expected on the floor (with a corresponding fining-downwards sequence at the roof) of a convecting system in which the sizes of all particles remain constant, it does not exhibit coarse-tail grading (Holness et al., 2017a). However, the population of particle sizes changes with time in a magmatic system, generally by nucleation and growth of individual crystals during cooling. Even at constant temperature, particles grow by the formation of grain clusters by synneusis (e.g. Schwindinger & Anderson, 1989; Philpotts et al., 1998, 1999; Schwindinger, 1999; Philpotts & Dickson, 2000; Wieser et al., 2019; Dyck & Holness, 2021), particularly in well-mixed convecting systems. Hence, the longer particles remain suspended in convecting magma, the larger they will be—individual grains will be larger due to continued growth, and clusters will be larger due to continued accretion. The progressive loss of particles from the convecting bulk magma, as they enter the lower boundary layer of the convection cell (Jaupart & Brandeis, 1986; Martin & Nokes, 1988; Patočka et al., 2022), will thus result in a coarsening-upwards sequence on the intrusion floor (involving both larger grains and larger clusters), and a corresponding coarsening-downwards sequence at the roof, formed as progressively larger particles brought up by convection currents get trapped in the downwards-propagating solidification front. This coarsening-downwards of the crystal cargo at the roof is critical evidence of vigorous convection—it cannot form during solidification of a static magma.

Other microstructural indicators of convection in basaltic systems are the spatial variation of shape and size of plagioclase grains. Under conditions of small undercooling, during which grain growth is controlled by the kinetics of attachment at interfaces (Kirkpatrick et al., 1976; Kirkpatrick, 1977; Cabane et al., 2005), plagioclase grains are tabular, flattened parallel to (010) (Muncill & Lasaga, 1987). These tablets are more equant in slowly cooled rocks compared to those in rapidly cooled rocks (Coish & Taylor, 1979; Holness, 2014), and, for rocks with no preferred grain orientation, this difference in shape can be straightforwardly detected using the average apparent aspect ratio (AR) of plagioclase (the arithmetic mean of the population of length/width ratios), as viewed in a thin section (Meurer & Boudreau, 1998; Boorman et al., 2004; Holness, 2014, 2015). Although AR cannot be used to quantify the range of true 3D grain shapes present in a sample, it is strongly correlated with the time taken to crystallise according to the relationship:

$$AR = 0.5586[6.34 - \log(\text{crystallisation time in years})],$$

where the crystallisation time is calculated assuming diffusive heat transport, a country rock temperature of 0°C, and a crystallisation interval of 1200–1000°C during which latent heat is released at a constant rate (Holness, 2014). AR therefore varies systematically in bodies in which solidification primarily involved *in situ* nucleation and growth at inwards-propagating solidification fronts (primarily sills), but is invariant across bodies (primarily dykes) in which the early stages of solidification involved the growth of crystals suspended in a convecting magma (Holness, 2014). Furthermore, while plagioclase grain size increases with increasing intrusion dimension, this increase is more sensitive to increasing intrusion width in dykes than in sills, with a narrower

range of grain sizes in dykes compared to sills (Philpotts & Ague, 2009; p. 85). Holness et al. (2017b) argue that this is also linked to differences in the location of crystal growth, with solidification front formation dominating in sills, and growth as suspended isolated grains in dykes.

Conversely, the cooling rate speedometer provided by the geometry of clinopyroxene-plagioclase-plagioclase three-grain junctions, as quantified by the median dihedral angle, Θ_{cpp} (Holness et al., 2012a), is not affected by the fluid dynamical regime during the early stages of crystallisation, because dihedral angles form during the last few vol% of solidification (Holness et al., 2012b). Hence, if crystallisation primarily occurred in solidification fronts, plagioclase grain shape, as quantified by AR, correlates with dihedral angle whereas in bodies in which solidification occurred in a range of different places, e.g. if significant plagioclase growth occurred as suspended grains in a convecting magma, plagioclase AR is decoupled from the dihedral angle (Holness et al., 2017b).

Arguments based on grain shape must take into account the possibility of progressive change during growth. The growth mechanism may change from interface-controlled to diffusion-limited, resulting in the evolution of initially equant crystals into skeletal forms as a compositional boundary layer develops (Hammer & Rutherford, 2002), and grains growing under interface-controlled conditions may change shape as they grow (Mangler et al., 2022). Furthermore, grain impingement during growth affects shape (Brown, 1956; Martin et al., 1987; Pupier et al., 2008 ; Schiavi et al., 2009 ; Applegarth et al., 2013). For grains growing with no preferred orientation, growth of closely spaced grains results in relatively equant shapes (i.e. lower AR) compared to those of the same mineral grown under conditions of low nucleation density (Martin et al., 1987). This is because impingement predominantly prevents growth on the faster-growing faces, so the earlier the impingement, the lower the final AR (Pupier et al., 2008; Schiavi et al., 2009; Applegarth et al., 2013). Impingement during crystallisation starts to affect plagioclase AR at volume fractions in the range 10–20 vol% (Pupier et al., 2008; Schiavi et al., 2009). Conversely, if crystals have a preferred alignment, adjacent grains are likely to be in contact on their slow-growing faces, resulting in an increasingly non-equant habit during continued growth (Brown, 1956).

GEOLOGICAL SETTING

The Little Minch Sill Complex, part of the Hebridean Igneous Province, is a stacked, multi-leaved Palaeocene group of dolerite sills, with its greatest onshore exposure on the coasts of the Trotternish Peninsula, Isle of Skye (e.g. Gibb & Gibson, 1989; Fyfe et al., 2021; Fig. 1). It intruded Mesozoic sediments and Palaeocene tuffs over an area of ~4000 km^2 (Fyfe et al., 1993) at a minimum depth of 3 km (Nicoli & Matthews, 2019). The thickness of individual sills in the complex varies between a few metres and >100 m, and many are composite (Gibson, 1988; Gibson & Jones, 1991; Gibb & Henderson, 1996; Schofield, 2009; Fyfe et al., 2021).

The magma filling the sills ranged from mildly alkaline picrite to picritic basalt, with a crystal cargo dominated by olivine, with small amounts of Cr-spinel and plagioclase (Gibb & Gibson, 1989; Gibb & Henderson, 1996, 2006). The observed range of bulk composition is almost entirely accounted for by variations in the amount of entrained olivine phenocrysts (Gibb & Henderson, 2006), enabling division into three lithologies (Gibb & Henderson, 1984): crinanite, picrodolerite and picrite. Crinanite is an analcime-bearing dolerite in which olivine is
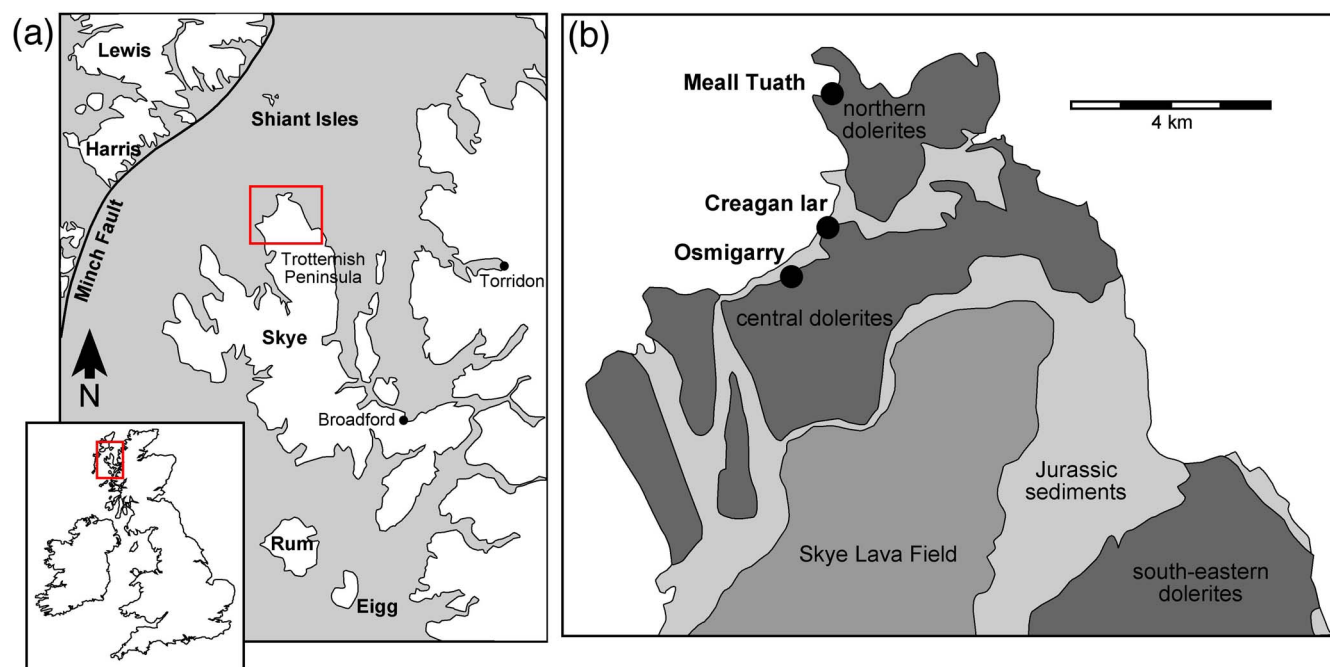
Figure 1. (a) The geographical setting of the Trotternish Peninsula and the Shiant Isles. The area enlarged in (b) is shown by the red rectangle. (b) A simplified geological map of the northern Trotternish Peninsula (from the 1:50000 map of the British Geological Survey), showing the location of the traverses across the composite sills at Creagan Iar and Meall Tuath.

predominantly ophitic: the transition to picrodolerite, in which olivine is predominantly euhedral to subhedral, is commonly placed at 15 vol% olivine (Gibb & Henderson, 1984) though occurs in the range 10–20 vol%. Picrite contains >40 vol% (euhedral) olivine (Gibb & Henderson, 1984). Many intrusions of the Little Minch Sill Complex comprise a lower picrodolerite that grades upwards into crinanite, interpreted as the result of cargo settling (Gibb & Gibson, 1989; Gibson & Jones, 1991; Gibb & Henderson, 1996; Gibb & Henderson, 2006).

In this contribution, we report the results of a microstructural examination of two composite sills of the Complex exposed on the Trotternish Peninsula, together with the picrodolerite-crinanite unit (PCU) of the composite Shiant Isles Main Sill, which was the focus of Holness et al. (2017a) (Fig. 1). We collected samples across vertical sections through the two Trotternish intrusions, maintaining approximately metric spacing between samples. Sample spacing was reduced in proximity to contacts.

ANALYTICAL METHODS

It is highly unlikely that all crystals in any particular sample will have the same shape (Duchêne et al., 2008; Iezzi et al., 2011)—for example, Mangler et al. (2022) showed a systematic change in the 3D shape of isolated plagioclase grains during progressive interface-controlled growth in glassy volcanic rocks. However, for fully solidified rocks with randomly oriented plagioclase grown under interface-controlled conditions, the average (arithmetic mean) apparent aspect ratio provides a first-order indication of how platy the grains are, with no assumptions about the true 3D shape or range of shapes required by other methods for quantifying grain shape from 2D sections (e.g. Higgins, 1994). A high average apparent aspect ratio observed in a rock with randomly oriented plagioclase correlates with a generally platy shape in 3D, while low AR correlates with a more equant shape: the usefulness of this simple measure of grain shape is demonstrated by its

strong correlation with the time taken to crystallise (Holness, 2014).

In this study, we confined our measurements to samples with randomly oriented plagioclase. The long and short axes of up to 330 plagioclase grains for each sample were drawn by eye on digital photographs of thin sections under crossed polars. The magnification was chosen such that all grains could be distinguished in the image, and all discernible grains were measured in each photograph, other than those grains truncated by the edge of the photograph. The smallest grains measured are ~40 microns long. The long and short axes were measured for each grain using the software package ImageJ to obtain the average apparent aspect ratio. The 2σ confidence interval on the average apparent aspect ratio was constrained using bootstrap sampling.

To facilitate comparison between the various intrusions of this study and those of previous related work we followed the approach of Holness (2014) and Holness et al. (2017a) and use the simplest measure of grain size (with no underlying assumptions about 3D grain shape or growth conditions), reporting both the average (arithmetic mean) and the skew (the adjusted Fisher–Pearson standardised moment coefficient) of the population of long axes of grain intersections as viewed in thin section.

Values of AR for the Creagan Iar and Meall Tuath sills were determined by amalgamating data obtained from a number of photomicrographs of each sample, but for the parts of the Shiant Isles Main sill PCU in which clinopyroxene is poikilitic we measured AR for the plagioclase chadacrysts in individual photomicrographs, each covering ~12 mm^2, to investigate the effect of impingement on plagioclase shape. We obtained values of AR for plagioclase outside the oikocrysts by amalgamating data from several photomicrographs.

We used the moment-based method of Farr et al. (2017) to determine the volume-weighted mean diameter, $D_{4,3}$, for individual olivine grains, clusters of olivine grains, and clusters formed of both olivine and pyroxene. For each sample, grain and

cluster intersection diameters were obtained by measuring the outline of phenocrysts and polycrystalline clusters, distinguishing between olivine-only, clinopyroxene-only and bi-mineralic (olivine + clinopyroxene) clusters. The area corresponding to the outline is then calculated using ImageJ software (Schneider et al., 2012) and converted to the equivalent circular grain intersection, i.e. the Heywood diameter.

The method of Farr et al. (2017) takes into account the change in average grain diameter of the crystal cargo caused by post-accumulation overgrowth to obtain the original volume-weighted mean diameter, $D^*_{4,3}$, of the olivine cargo (c.f. Holness et al., 2017a). This correction was performed for olivine phenocrysts and olivine-only clusters, but not for olivine clusters surrounded by a rim of heterogeneously nucleated clinopyroxene. To measure the overall size of these bi-mineralic clusters, we corrected for post-settling overgrowth of the clinopyroxene by ignoring the irregular interstitial overgrowth of initially euhedral grains. A similar approach was used for clinopyroxene-only clusters and also for olivine-only clusters in relatively olivine-poor samples (e.g. MT34, MT35, MT36 and MT38; Table 2) in which some clusters display late, irregular olivine overgrowth with no clinopyroxene corona present in the plane of the section.

Clinopyroxene-plagioclase-plagioclase dihedral angles were measured using a Leitz 4-axis universal stage mounted on an optical microscope, with a ×32 long working distance objective (the eyepiece adds a further ×10 magnification). Between 40 and 70 measurements were made on each sample to determine the median value, Θ_{cpp}, of the population of true 3D dihedral angles, with the 95% confidence interval about the median calculated following Stickels & Hücke (1964). Holness et al. (2005) found higher median dihedral angles at the three-grain junctions formed by clustered olivine chadacrysts enclosed in pyroxene oikocrysts in the centres of the oikocrysts compared to the edges (which they attributed to post-enclosure textural equilibration), so we confined our measurements of Θ_{cpp} to the edges and exterior of oikocrysts in samples containing poikilitic clinopyroxene.

PETROGRAPHY AND MICROSTRUCTURAL ANALYSIS
The Shiant Isles Main Sill

The Shiant Isles Main sill is the most studied intrusion of the Little Minch Sill Complex (Gibb & Henderson, 1984, 1992, 1996, 2006, 2014; Gibb & Gibson, 1989; Foland et al., 2000; Latypov & Chistyakova, 2009; Latypov, 2014; Holness et al., 2017a) and is thought to have been fed via the Minch Fault (Fig. 1; Fyfe et al., 2021). It comprises four separate intrusions (Gibb & Henderson, 1996), the larger two of which are a 24-m picrite intrusion (forming the base of the composite body) and an overlying later 135-m-thick PCU characterised by a pronounced basal concentration of olivine primocrysts (Fig. 2). Here, we focus on the 135-m-thick PCU.

The olivine grain size in the basal picrodolerite of the PCU decreases upwards through the lowermost 10 m but then increases upwards through the remaining ~50 m (Holness et al., 2017a). Holness et al. (2017a) argued that the fining-upwards sequence formed by settling of most of the olivine cargo shortly after emplacement. The overlying coarsening-upwards sequence formed by accumulation of olivine grown post-emplacement in a strongly convecting magma, with a progressive increase in cluster size due to synneusis. The case for convection during solidification is strengthened by the mirroring of the

coarsening-upwards sequence on the floor by a coarsening-downwards sequence at the roof, in which the size of both individual grains and of grain clusters reaches values similar to that of the coarsest-grained horizons of the floor accumulation (Holness et al., 2017a), in stark contrast to the fining-downwards antecryst distributions expected at the roof of static magma bodies (Marsh, 1988).

Both olivine and clinopyroxene in the crinanite, between ~80 m and 150 m stratigraphic height in the composite intrusion (Gibb & Henderson, 1996; Gibb & Henderson, 2006), form large oikocrysts enclosing a framework of plagioclase grains (Fig. 3a, b). These frameworks are highly reminiscent of those described by Philpotts et al. (1998, 1999) and Philpotts & Dickson (2000) and ascribed to synneusis. The olivine oikocrysts enclose a greater proportion of plagioclase than do the pyroxene oikocrysts. The size of the clinopyroxene oikocrysts increases with height, exceeding 2 cm (i.e. the dimensions of thin sections) at 100–120 m. The amount of plagioclase enclosed by the clinopyroxene oikocrysts varies, with a minimum of 40 vol% in the compositionally uniform cores increasing towards the (commonly compositionally zoned) oikocryst margins to values typical of that in the olivine oikocrysts. These observations are consistent not only with the centres of the pyroxene oikocrysts recording the earliest history of framework formation (e.g. Mathison, 1987; Higgins, 1998), with open frameworks collapsing and densifying where not preserved by enclosure, but also with relatively rapid early growth of interstitial clinopyroxene compared to the associated interstitial olivine.

The regions between oikocrysts are dominated by plagioclase (Fig. 3c). Fe-Ti oxides are interstitial in the lower parts of the PCU (below ~81 m height) and in the matching upper parts of the intrusion (above ~140 m) and occur only outside oikocrysts (Figs 3b, c). In the more evolved, central parts of the sill, oxides are euhedral, with some hopper grains (Fig. 3d) in the margins of the clinopyroxene oikocrysts.

The median clinopyroxene-plagioclase-plagioclase dihedral angle, Θ_{cpp}, forms a broadly W-shaped profile through the PCU with a maximum of 65–70 m and marginal reversals creating minima at ~30 and 150 m (Holness et al., 2017a; Fig. 2 and Supplementary Appendix 1). The observed values are within error of the expected values (calculated following Holness et al., 2012a) in the picrodolerite (with the exception of the lowest few metres), but those in the crinanite are significantly lower than expected values (Fig. 2).

In those parts of the PCU in which olivine forms compact grains, and in which interstitial clinopyroxene is not notably poikilitic (i.e. below about 50 m stratigraphic height in the composite intrusion), the average apparent aspect ratio of plagioclase is the same inside and outside the (poorly developed) oikocrysts (Table 1). With increasing height in the PCU, these values begin to diverge, with higher values of aspect ratio in the oikocrysts (Fig. 2). In samples with strongly poikilitic clinopyroxene, there is a negative correlation between AR of the plagioclase chadacrysts and the mode of those chadacrysts as measured in single photomicrographs (Fig. 4). This is particularly evident when data from sample S81/35 (at 100.86 m stratigraphic height) are considered: the clinopyroxene in this sample forms a sufficient area of oikocrysts to permit measurement of seven non-overlapping 4.5 × 3 mm areas, for comparison with plagioclase grain shape outside the oikocrysts (Table 1; Fig. 4).

Both the maximum value of local AR and the range of AR seen in individual photomicrographs from any sample through the crinanite increase with height, reaching their maximum values at ~120 m in the composite sill, close to the sandwich horizon
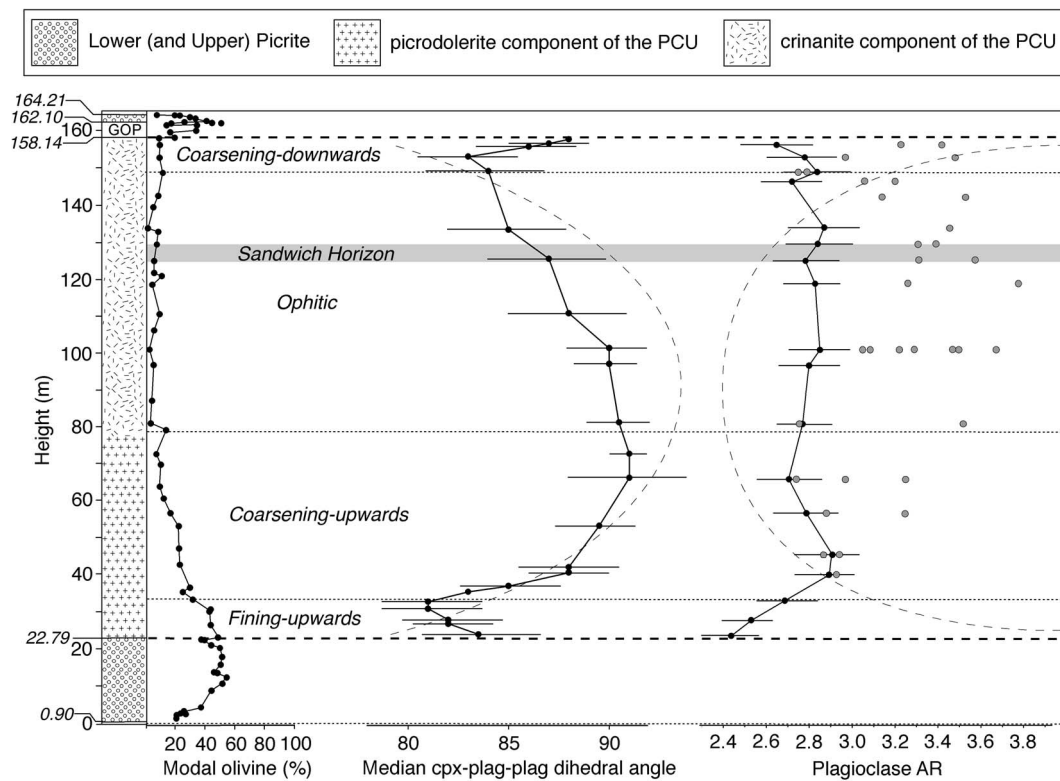
Figure 2. The stratigraphy of the Shiant Isles Main sill (simplified from Gibb & Henderson, 1996). The abbreviation GOP shows the stratigraphic location of the last-to-intrude Granular Olivine Picrodolerite component of the composite sill (see Gibb & Henderson, 1996, for details). The approximate position of the sandwich horizon is estimated from the stratigraphic position of the most evolved rocks (from Gibb & Henderson, 2006). The labels in italics give the microstructural habit of the olivine. Also shown is the variation in olivine mode (from Henderson et al., 2000), the median value of the clinopyroxene-plagioclase-plagioclase dihedral angle (from Holness et al., 2017a), and the average apparent aspect ratio (AR) of the plagioclase in the PCU. The AR data shown by the black dots refer to plagioclase outside clinopyroxene oikocrysts, whereas the grey dots show values pertaining to the plagioclase chadacrysts in single photomicrographs (each covering 4.5 × 3 mm area of thin section) dominated by oikocrysts (those data points in the crinanite are also shown in Fig. 2). The dashed lines on the plots of dihedral angle and AR show the expected values of these two parameters for a sill with a thickness of 135 m, calculated according to the data compilations of Holness et al. (2012a) and (2014), respectively.

(Table 1; Fig. 2). In contrast, the shape of plagioclase grains that are not enclosed by oikocrysts is much less variable: AR increases upwards over ~20 m from a minimum of ~2.4 at the base of the PCU to between ~2.8 and 3.0 through the remainder of the PCU, remaining essentially constant within error, and significantly lower than the values found for localised areas enclosed by oikocrysts (Fig. 2). This is also evident from Fig. 4, which shows that AR reaches a relatively constant value once the mode of plagioclase exceeds ~65 vol%. There is no correspondence between the observed values of AR and those expected for a dolerite sill of 135 m thickness, shown by the dotted line in Fig. 2, which was calculated assuming the 135-m-thick sill was a single body intruded into cold country rock and using the observed variation of AR with calculated crystallisation time of Holness (2014).

The average long axis of plagioclase grains outside oikocrysts increases through the PCU, from a minimum of ~0.17 mm to 0.28 mm (Table 1; Supplementary Appendix 2), similar to values observed in sills of this thickness by Holness et al. (2017b). The frequency distribution of values of the skew of the grain length populations is also similar to that reported for sills by Holness et al. (2017b) (Fig. 5).

The Meall Tuath sill

The composite Meall Tuath sill is the thickest of the sills exposed on the Trotternish Peninsula, forming a sheer cliff face (Fig. 6a–c) and belonging to the northern dolerites as defined by Schofield

(2009). It was fed from a magma source to the south-east (Schofield, 2009). Although the top contact is above the present erosion surface, local topography suggests it is likely to be between 100 and 110 m thick, consistent with abundant field evidence for the exposed top surfaces of the Trotternish sills being at, or close to, their upper contacts (Schofield, 2009). The Meall Tuath sill comprises an early PCU (of which the lower ~48 m is exposed), and a later, ~50 m thick, picrite sill that intruded into the lower part of the PCU (Gibson, 1988), some 5 m above its lower contact (Fig. 6a). The later picrite has well-developed chilled margins against the enclosing PCU (Fig. 6a), with decreasing spacing of columnar jointing towards the contacts (Schofield, 2009), suggestive of significant cooling of the earlier PCU before the picrite was intruded. Here, we focus on the older of the two components of this composite intrusion: the stratigraphic heights given in the remainder of this contribution omit the later picrite.

The basal chilled margin of the Meall Tuath PCU is in contact with Jurassic sediments and contains ~30 vol% euhedral olivine phenocrysts (Fig. 7a) and small, euhedral, included grains of chromite (Nicoli & Matthews, 2019). Clusters of up to 10 grains (as viewed in thin section) are present in the chill, attesting to the presence of clusters in the crystal cargo. There are no phenocrysts of other phases. The immediately overlying picrodolerite contains abundant euhedral olivine grains and grain clusters. The olivine mode increases sharply from 11 vol% in the lowest cm, to 46 vol% 1 m from the base (Table 2). It then decreases steadily upwards,
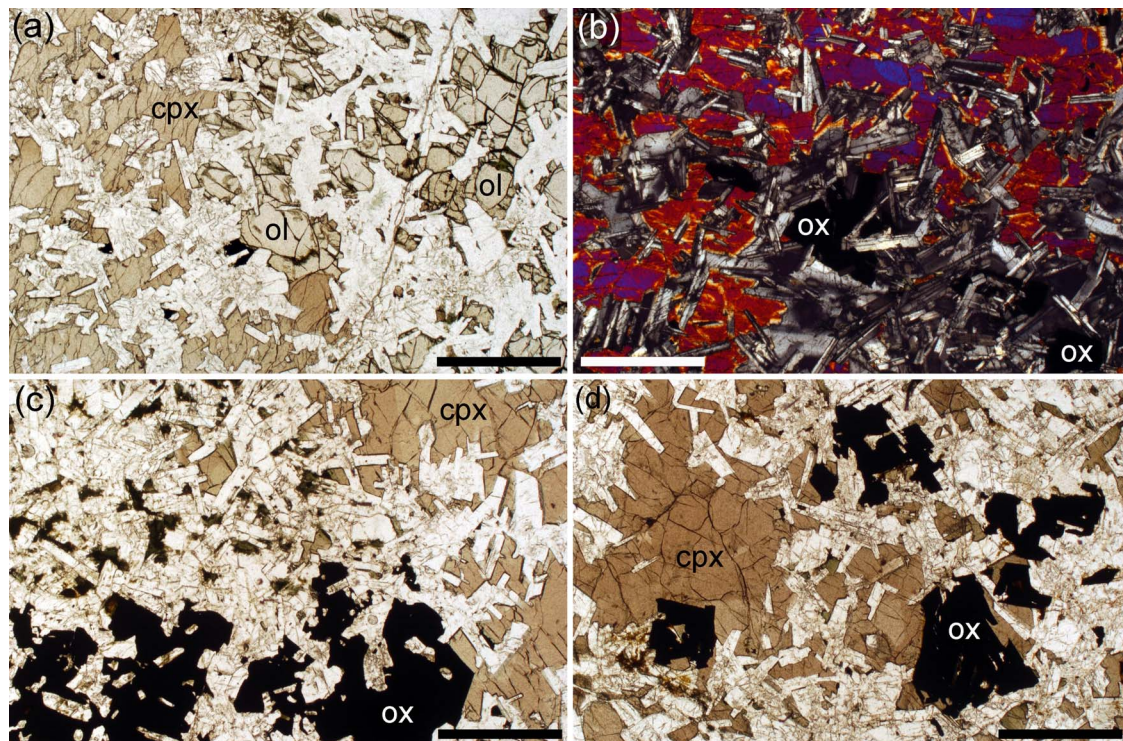
Figure 3. Photomicrographs of the crinanite part of the Shiant Isles Main sill PCU. All scale bars are 1 mm long. (a) Sample S82/68 (from 120.73 m stratigraphic height in the composite intrusion). The left half of the image comprises an oikocryst of clinopyroxene, while the right half is an olivine oikocryst. Both contain abundant plagioclase inclusions, but the olivine generally contains more plagioclase than does the clinopyroxene. (b) Sample S82/67 (from 118.6 m stratigraphic height in the composite intrusion). Note the framework of plagioclase grains preserved inside the clinopyroxene oikocryst. Oxide is found only outside the clinopyroxene oikocrysts, in regions dominated by plagioclase. (c) Sample SC1191 (from 146.2 m stratigraphic height in the composite intrusion). Oxide is an interstitial phase in the relatively primitive crinanite far from the sandwich horizon. (d) Sample S82/69 (from 132.92 m height in the composite intrusion). Oxides grains are more equant and generally compact, although some display irregularities indicative of hopper-style (diffusion-limited) growth.

with an abrupt drop to ~10 vol% some 20 m above the base, followed by a slow decrease of a few vol% in the overlying 15 m (Fig. 8). The olivine mode then increases in the uppermost 10 m of the exposure, to a maximum of 15 vol%, forming a poorly defined S-type profile (c.f. Marsh, 1988), with clearly identifiable olivine primocrysts and clusters present in the topmost three samples of our traverse.

The grain size of individual olivine grains in the lower 20 m of the PCU is generally constant (Table 2). However, the size of olivine clusters increases from the lowest horizon where they can be easily differentiated from each other, at ~5 m stratigraphic height, to a maximum at ~10 m height (Fig. 8). Cluster size may decrease upwards through the remaining picrodolerite, although this decrease is defined by only two data points. The size of both individual olivine grains and olivine clusters is smaller in the topmost three samples of our traverse compared to that in the lower part of the sill.

Clinopyroxene forms oikocrysts in the picrodolerite (Fig. 7b), enclosing both plagioclase and olivine: the size of these oikocrysts (and the number of plagioclase inclusions) increases up-stratigraphy to a maximum of ~5 mm diameter before an abrupt transition to small (~0.25 mm diameter), equant, inclusion-free grains between 8.5 m and 9.1 m from the base (Fig. 7c). These fine grains commonly form clusters. Significantly, these equant clinopyroxene grains are commonly attached to, and may entirely surround, olivine primocrysts (Fig. 7c). Although Gibson & Jones (1991) suggest these pyroxene mantles may have formed by reaction of olivine with the surrounding liquid, we consider them more likely to be a consequence of heterogeneous

nucleation on the olivine substrate of pyroxene crystallising directly from the evolving liquid. That there was no peritectic reaction involving olivine is supported by the presence of compact grains of clinopyroxene within grain clusters dominated by olivine.

Clinopyroxene is exclusively represented by clusters of small equant grains for at least 4 m of stratigraphy, but above ~18 m stratigraphic height, the number and size of the clusters of equant grains drops significantly. Instead of ~90% of the pyroxene forming clusters of small equant grains, each thin section contains ~10 clusters comprising few grains (in the plane of the section), with most of the pyroxene forming large (~3 mm in diameter at ~20 m height) isolated grains (Fig. 7d), with abundant inclusions of plagioclase and highly irregular margins, indicative of interstitial growth (Fig. 7e). The few remaining clusters of small, inclusion-free, equant grains are invariably surrounded by these large, inclusion-rich grains (Fig. 7d, e), suggestive of extensive interstitial overgrowth of the outer grains of a cluster: olivine is a rare component of these clusters. The number of clusters of small compact grains continues to decrease with stratigraphic height, with only a few small clusters present on the thin section scale at 35 m. Instead, pyroxene forms large oikocrysts (Fig. 7e). Pyroxene clusters re-appear above ~44 m, but are relatively rare and occur in the centres of large groups of oikocrysts (c.f. Fig. 7e). The ratio of pyroxene to plagioclase is greatest at 37 m height, which is therefore likely to be the sandwich horizon.

Given that the settling behaviour of the olivine clusters is affected by the amount of heterogeneously nucleated clinopyroxene on their margins, we re-calculated the average size of the

Table 1: The stratigraphic variation of plagioclase grain shape and size as a function of height in the PCU of the Shiant Isles Main Sill

Sample	Height (m)	n	vol% plag	Plagioclase grain size		Average apparent aspect ratio (AR)			
				Average (mm)	Skew	Chadacrysts	Outside oikocrysts	Min	Max
SC518	23.63	229		0.25	1.87		2.44	2.30	2.57
SC482	27.61	215		0.23	1.27		2.53	2.39	2.64
S81/10	32.95	282		0.17	1.50		2.69	2.55	2.84
S81/15	39.95	162		0.21	1.44	2.93		2.76	3.09
		392					2.89	2.73	3.01
		150				2.87		2.71	3.04
S81/19	45.57	149		0.20	1.18	2.94		2.77	3.09
		268					2.91	2.74	3.04
		130	53.7			3.25		3.05	3.36
S81/24	56.57	128	40.4	0.21	2.40	2.88		2.75	2.99
		288	67.2				2.79	2.63	2.93
		102	51.5			2.97		2.82	3.15
S81/27	65.87	147	54.0	0.21	1.22	3.25		3.09	3.41
		185	52.0			2.74		2.60	2.88
		251	71.5				2.71	2.56	2.86
		106	56.3			3.52		3.19	3.62
S81/32	80.80	128	43.4	0.24	0.72	2.76		2.60	2.92
		255	69.8				2.76	2.72	3.02
S81/34	96.95	223					2.8	2.66	2.95
		159	49.0			3.50		3.27	3.72
		146	62.0			3.09		2.84	3.22
		143	58.0			3.22		3.01	3.43
S81/35	100.86	191	61.0	0.26	1.25	3.05		2.88	3.27
		154	50.0			3.47		3.20	3.68
		108	49.0			3.67		3.33	4.04
		161	52.0			3.29		3.11	3.44
		222	69.4				2.85	2.71	2.99
		128	44.2			3.26		3.05	3.45
		93	59.3	0.28	1.23	3.77		3.57	4.01
S82/67	118.60	312	73.4				2.83	2.68	2.94
		97	44.0			3.31		3.10	3.49
SC1464	125.02	105	44.8	0.27	1.30	3.57		3.34	3.77
		227	78.3				2.78	2.63	2.94
		104	48.3			3.39		3.16	3.57
		103	41.8	0.27	2.60	3.31		3.09	3.50
SC1397	129.36	282	80.0				2.84	2.67	3.01
		68	59.7			3.46		2.57	2.99
SC1337	133.73	106	57.0	0.28	2.25	3.45		3.09	3.50
		258	65.4				2.87	2.70	3.04
		70	56.9			3.06		2.90	3.21
SC1191	146.20	109	48.4	0.28	2.67	3.20		3.00	3.37
		264	71.2				2.72	2.58	2.86
		128	49.7			2.79		2.66	2.96
SC1160	148.71	130	69.7	0.26	1.08	2.75		2.59	2.87
		299	84.2				2.84	2.68	3.00
SC1131	152.63	103	49.2	0.28	1.18	3.48		3.23	3.71
		332	79.5				2.78	2.60	2.93
		139	49.5			3.23		2.99	3.45
SC1081	156.16	118	39.4	0.24	1.48	3.42		3.14	3.67
		329	71.0				2.65	2.48	2.82

The number of individual grains measured is given by *n*, with multiple values of both *n* and the vol% of plagioclase denoting individual photomicrographs of chadacrysts taken for a single sample. Plagioclase grain size was averaged using all grains measured for each sample. Values of AR for chadacrysts were measured in single photomicrographs (4.5 × 3 mm). The min and max values give the 2σ uncertainties for the average value.

clusters to include the attached clinopyroxene grains (Table 2). These averages, presented in Fig. 8, also include the size of clusters of equant, compact clinopyroxene grains (with no olivine visible in the plane of the thin section). The average size of clusters of olivine ± clinopyroxene and clinopyroxene only, are the same within error as those of olivine alone (Table 2; Fig. 8).

Fe-Ti oxides form isolated euhedral grains and grain clusters through the traverse, attesting to nucleation and growth in a liquid-rich environment. While ilmenite commonly forms elongate grains, magnetite grains exhibit an open, facetted, structure with crystallographic branching indicative of diffusion-limited growth (Fig. 7f). The complexity of dendritic growth morphology, and the size of individual grains, increases with stratigraphic height (from 0.05 mm to 0.5 mm in diameter). Small quantities of highly altered interstitial analcime are present throughout the traverse.

Table 2: The stratigraphic variation of microstructure in the PCU of the composite Meall Tuath Sill

Sample	Height (m)	vol% olivine	Θ_{cpp}	Olivine grain size			Olivine-only clusters			Bi-mineralic clusters			Plagioclase grain size		Plagioclase grain shape			
				n	$D_{4,3}$	σ	n	$D_{4,3}$	σ	n	$D_{4,3}$	σ	Average (mm)	Skew	n	AR	Min	Max
MT36	47.1	20.3	81.5 ± 3	53	0.5	0.07	11	0.81	0.11	25	0.84	0.11	0.153	1.468	271	3.28	3.13	3.41
MT35	45.6	17.3	-	26	0.36	0.09	9	0.69	0.12	19	0.64	0.08	0.204	2.478	273	3.22	3.05	3.37
MT34	43.6	19.4	85 ± 2	31	0.35	0.05	11	0.63	0.06	16	0.64	0.07	0.132	2.305	273	3.21	3.03	3.38
MT33	42.6	16.5	-	-	-	-	-	-	-	-	-	-	-		-	-	-	-
MT28	40.1	14.75	86 ± 2.5	-	-	-	-	-	-	-	-	-	0.165	1.899	252	3.03	2.87	3.21
MT27	37.8	12.1	-	-	-	-	-	-	-	-	-	-	0.170	2.259	225	3.09	2.95	3.25
MT26	36.6	9.2	88 ± 2	-	-	-	-	-	-	-	-	-	0.151	2.201	271	2.86	2.71	3.02
MT25	32.1	9.4	-	-	-	-	-	-	-	-	-	-	-		-	-	-	-
MT09	29.1	9.6	89.5 ± 2.5	-	-	-	-	-	-	-	-	-	0.141	1.688	330	2.77	2.64	2.89
MT10	27.1	9.3	-	-	-	-	-	-	-	-	-	-	0.138	1.363	283	2.65	2.52	2.79
MT11	23.6	9.4	88 ± 2.5	-	-	-	-	-	-	-	-	-	0.131	2.105	253	2.77	2.61	2.89
MT12	21.1	11.2	-	-	-	-	-	-	-	-	-	-	0.150	1.711	254	2.85	2.7	2.95
MT13	19.6	11.5	88 ± 2	-	-	-	-	-	-	-	-	-	-		-	-	-	-
MT14	17.8	21.0	-	149	0.97	0.10	27	1.85	0.39	50	1.82	0.21	0.129	2.301	298	2.63	2.5	2.73
MT15	13.3	22.0	87 ± 3	259	0.96	0.08	89	1.96	0.35	95	1.93	0.32	0.138	1.144	222	2.91	2.77	3
MT16	11.0	24.0	-	277	1.27	0.14	69	2.3	0.34	86	2.38	0.35	0.342	1.413	251	2.83	2.67	2.98
MT38	9.1	30.0	-	380	0.88	0.06	98	1.65	0.16	105	1.69	0.14	-		-	-	-	-
MT17	8.5	29.0	87 ± 2.5	278	0.84	0.06	64	1.57	0.15	-	-	-	0.126	1.191	294	3.02	2.89	3.2
MT29	6.0	30.1	87 ± 2	260	0.79	0.08	70	1.19	1.19	-	-	-	0.122	2.255	293	2.95	2.82	3.06
MT18	5.1	31.5	83 ± 2	310	0.75	0.04	47	1.56	1.56	-	-	-	0.132	1.720	225	3.14	2.99	3.3
MT6b	4.5	30.0	83 ± 3	324	0.82	0.04	-	-	-	-	-	-	-		-	-	-	-
MT05	3.95	32.8	-	255	0.88	0.05	-	-	-	-	-	-	0.291	1.384	225	3.255	3.09	3.42
MT04	2.9	39.0	83 ± 2	299	0.70	0.03	-	-	-	-	-	-	-		-	-	-	-
MT03	1.8	46.0	-	333	0.61	0.03	-	-	-	-	-	-	0.289	0.886	299	3.39	3.19	3.57
MT02	1.0	46.0	78.5 ± 3.5	347	0.82	0.05	-	-	-	-	-	-	0.182	0.769	248	3.87	3.7	4.05
MT01b	0.05	25.0	-	256	0.93	0.05	-	-	-	-	-	-	-		-	-	-	-

The heights given omit the later intruded picrite. The median value of the clinopyroxene-plagioclase-plagioclase dihedral angle is given by Θ_{cpp}. The number of grains measured is given by n. The volume-weighted mean diameter of individual olivine grains and grain clusters (both olivine-only and olivine-clinopyroxene), $D_{4,3}$, was calculated according to the method of Farr et al. (2017). The minimum and maximum values of average apparent aspect ratio (AR) show the 2σ confidence intervals around the mean.

Plagioclase has an average grain length of ~0.13–0.20 mm through much of the Meall Tuath PCU, with the exception of two samples rich in olivine cargo, which contain relatively elongate plagioclase (average lengths of ~0.3 mm), and a single sample at 11 m stratigraphic height (Table 2). The average grain size is similar to that expected for a sill of this thickness (Holness et al., 2017b), and the skew of the long axis populations is similar to that reported for sills by Holness et al. (2017b) (Fig. 5). AR of plagioclase outside clinopyroxene oikocrysts describes a U-shape through the intrusion, with a maximum value of 3.87 at the base, decreasing to a minimum of 2.65 at ~27 m before increasing upwards (Fig. 8). The expected values of AR, calculated for a range of sill thickness from 50 to 70 m using the relationship between observed AR and calculated crystallisation time of Holness (2014), are also shown in Fig. 8. The observed AR values are lower than the expected values in the lower half of the stratigraphy, but fall between values expected for a sill thickness of 60 and 70 m in the upper half.

The median clinopyroxene-plagioclase-plagioclase dihedral angles through the Meall Tuath PCU broadly describe a U-shape in the opposite sense to that of AR (Fig. 8). In detail, instead of the smooth stratigraphic variation of Θ_{cpp} expected for a non-fractionating body, there is a marked step-wise increase between 5.1 and 6 m height, and the high values in the central part of the sill are, within error, constant before the decrease to lower values at the top of the traverse. Values at the top of the traverse are consistent with a total thickness of 50–60 m, but are higher than the calculated curves in the lower part of the PCU. There is no variation of Θ_{cpp} either immediately below, or above, the later picrite.

The Creagan Iar sill

The composite Creagan Iar sill is at least 90 m thick and belongs to the central dolerites as defined by Schofield (2009) (Fig. 1), intruded at a higher stratigraphic level than the northern dolerites but fed from the same source to the south-east (Schofield, 2009; Fyfe et al., 2021). The lower contact with the underlying Jurassic sediments is not exposed but can be constrained to within a few tens of metres, whereas the upper part of the sill is absent (Fig. 6d). Our samples are derived from ~25 m of almost continuous exposure, found some 70 m above the base of the composite intrusion and including the contact between a lower picrite and the basal ~16 m of an overlying PCU (Fig. 6e). Earlier work reported an internal chilled margin within the upper crinanite at ~93 m stratigraphic height (Gibson, 1988; Gibson & Jones, 1991; stratigraphic heights as given in Fig. 9), but we did not find this and treat the Creagan Iar PCU as a single intrusion.

The distinction in the field between the different magma batches is less straightforward than for the Meall Tuath sill. Along strike, ~1.5 km to the west at Osmigarry (Fig. 1), a lower picrite is separated from an overlying PCU by a screen of Jurassic sediments (Gibson & Jones, 1991). At Creagan Iar, there is a marked change in slope corresponding to the picrite-picrodolerite transition (c.f. Schofield, 2009; Fig. 6d), although in outcrop the contact is diffuse (Walker, 1931). Columnar jointing runs through the entire body (Fig. 6e), consistent with a short time separating the two intrusive episodes. Although there is a clear distinction between the two bodies on the basis of olivine mode and grain size (Fig. 9), the absence of chilled margins, together with the incomplete record of
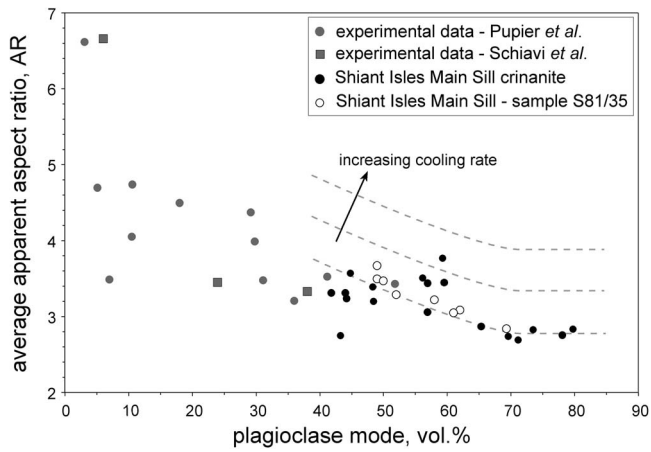
Figure 4. The variation of average apparent aspect ratio (AR) of plagioclase as a function of progressive solidification. The experimental data, plotted as a function of vol% total solids (of which plagioclase is predominant), are taken from Pupier et al. (2008) and Schiavi et al. (2009). The data from the Shiant Isles Main Sill crinanite (above 80 m stratigraphic height) are plotted as a function of plagioclase mode. The data for plagioclase chadacrysts are determined from a single photomicrograph (covering 4.5 × 3 mm area of thin section containing only plagioclase and clinopyroxene), whereas that for plagioclase outside the oikocrysts is averaged over several photomicrographs (data in Table 1). Sample S81/35 contained sufficient oikocrysts to enable the collection of eight data points (seven for chadacrysts and one for plagioclase outside the oikocrysts), and these are differentiated from the others to show the negative correlation between plagioclase grain shape and the progressive crystallisation of plagioclase within a single thin section. The dotted lines show suggested possible trajectories for systems with different cooling rates: the lines are shifted to higher values of AR as the cooling rate increases.

internal contacts, means that it is not straightforward to establish their relative age.

The picrite is dominated by olivine primocrysts, with an upwards decreasing mode through our sample traverse (Table 3; Fig. 9). The base of the overlying PCU also contains abundant grains and clusters of olivine, with many of the olivine grains containing small euhedral chromite inclusions. The olivine mode is highest within a few metres of the base, and decreases upwards from a maximum of 46–10 vol%, consistent with an overall S-type modal distribution (Table 3; Fig. 9). Although the olivine mode in our topmost two samples is that of a crinanite according to Gibb & Henderson (1984), the olivine is not interstitial: it is not directly analogous to the Shiant Isles Main sill crinanite. The average size of individual olivine grains coarsens upwards in the lowest 5 m, followed by a rapid decrease over a few metres to ~0.8 mm— grains are all this size to the top of our traverse. If we consider only clusters formed of olivine grains, these coarsen upwards from the base of the PCU until about 87 m height, above which the average cluster size decreases, approaching that of individual grains (i.e. clusters contain only a few grains). The full picture of cluster size variation, however, requires us to also consider the behaviour of clinopyroxene.

Clinopyroxene is interstitial at the base of the Creagan Iar PCU, commonly with inclusion-free cores: any included plagioclase grains may be significantly larger than those outside (Fig. 10a). The same abrupt transition observed in the Meall Tuath PCU, from oikocrysts to small, equant, grain clusters, occurs at Creagan Iar between 87.6 m and 88.3 m. In a similar fashion to the Meall Tuath dolerites, clinopyroxene and olivine form bi-mineralic clusters (Fig. 10b), and individual olivine grains and clusters are commonly

Table 3: The stratigraphic variation of microstructure in the composite Creagan Iar sill

Sample	Height (m)	vol% olivine	Θcpp	Olivine grain size n	Olivine grain size D4,3	Olivine grain size σ	Olivine-only clusters n	Olivine-only clusters D4,3	Olivine-only clusters σ	Bi-mineralic clusters n	Bi-mineralic clusters D4,3	Bi-mineralic clusters σ	Plagioclase grain size Average (mm)	Plagioclase grain size Skew	Plagioclase grain shape n	Plagioclase grain shape AR	Plagioclase grain shape Min	Plagioclase grain shape Max
PCU																		
CI18	97.0	13.9	87.5±3.5	99	0.80	0.26	44	1.10	0.22	98	1.44	0.22	0.237	1.458	254	2.59	2.41	2.71
CI17	96.0	10.1	-	74	0.65	0.14	33	0.96	0.16	78	1.38	0.22	0.261	1.530	252	2.55	2.4	2.65
CI1	94.6	17.1	86±2	86	0.79	0.12	34	1.16	0.17	66	1.69	0.31	0.250	1.390	312	2.72	2.57	2.84
CI2	92.6	17.0	-	210	0.80	0.10	54	1.35	0.18	82	1.63	0.19	0.244	1.791	210	2.7	2.58	2.82
CI3	91.3	23.0	84±2	245	0.93	0.17	85	1.51	0.27	98	1.66	0.28	-	-	-	-	-	-
CI4	90.3	24.0	-	343	0.83	0.09	114	1.68	0.32	110	1.84	0.34	-	-	-	-	-	-
CI5	89.6	24.5	82±2.5	267	1.02	0.08	91	1.99	0.24	92	2.31	0.34	0.219	1.799	279	2.61	2.48	2.75
CI6	88.3	23.7	-	257	0.93	0.08	71	1.65	0.13	77	1.92	0.20	-	-	-	-	-	-
CI6b	87.6	25.5	84±2	145	1.36	0.16	32	2.02	0.24	-	-	-	0.253	1.348	212	2.61	2.49	2.7
CI7	86.7	45.0	-	186	1.22	0.16	21	3.38	0.74	-	-	-	-	-	-	-	-	-
CI8	86.0	44.0	-	154	1.08	0.14	26	2.58	0.59	-	-	-	0.186	1.255	263	2.63	2.51	2.74
CI9	85.1	42.0	86.5±2.5	250	0.86	0.06	48	2.08	0.34	-	-	-	-	-	-	-	-	-
CI10	83.1	33.7	90±2.5	213	0.95	0.10	35	1.93	0.23	-	-	-	0.225	1.579	257	2.64	2.49	2.78
Underlying picrite																		
CI11	82.2	28.2	-	193	1.21	0.12	-	-	-	-	-	-	-	-	-	-	-	-
CI12	81.1	31.5	-	171	1.31	0.11	-	-	-	-	-	-	-	-	-	-	-	-
CI13	79.2	36.8	-	125	1.55	0.11	-	-	-	-	-	-	-	-	-	-	-	-
CI15	76.6	39.35	-	134	1.90	0.25	-	-	-	-	-	-	-	-	-	-	-	-
CI16	71.8	44.35	-	153	1.36	0.07	-	-	-	-	-	-	-	-	-	-	-	-

The height is that above the base of the composite sill. The median value of the clinopyroxene-plagioclase-plagioclase dihedral angle is given by Θcpp. The number of grains measured is given by n. The volume-weighted mean diameter of individual olivine grains and grain clusters (both olivine-only and olivine-clinopyroxene), D4,3, was calculated according to the method of Farr et al. (2017). The minimum and maximum values of AR show the 2σ confidence intervals around the mean.
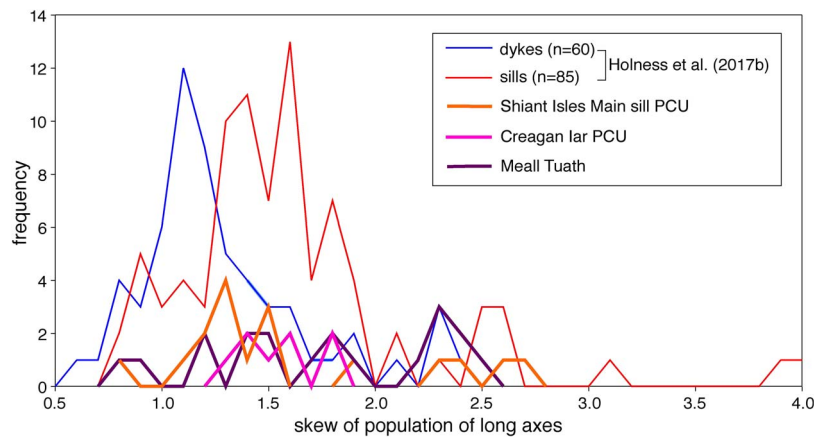
Figure 5. The frequency distribution of values of skew of the population of plagioclase long axes. The distributions of skew in dykes and sills from Holness et al. (2017b) are shown. Plagioclase shape in the dykes is invariant and is associated with a generally coarser grain size relative to sills, while shape in sills varies with stratigraphic height. The difference in grain size population between dykes and sills is attributed to vigorous and long-lived convection in the former, with plagioclase growth confined to inwards-propagating solidification fronts in non-convecting sills (Holness et al., 2017b). The frequency distribution of skews in the Shiant Isles Main sill PCU and the Creagan Iar and Meall Tuath sills are similar to those found in sills by Holness et al. (2017b), despite the arguments we propose in support of long-lived convection in these three bodies.
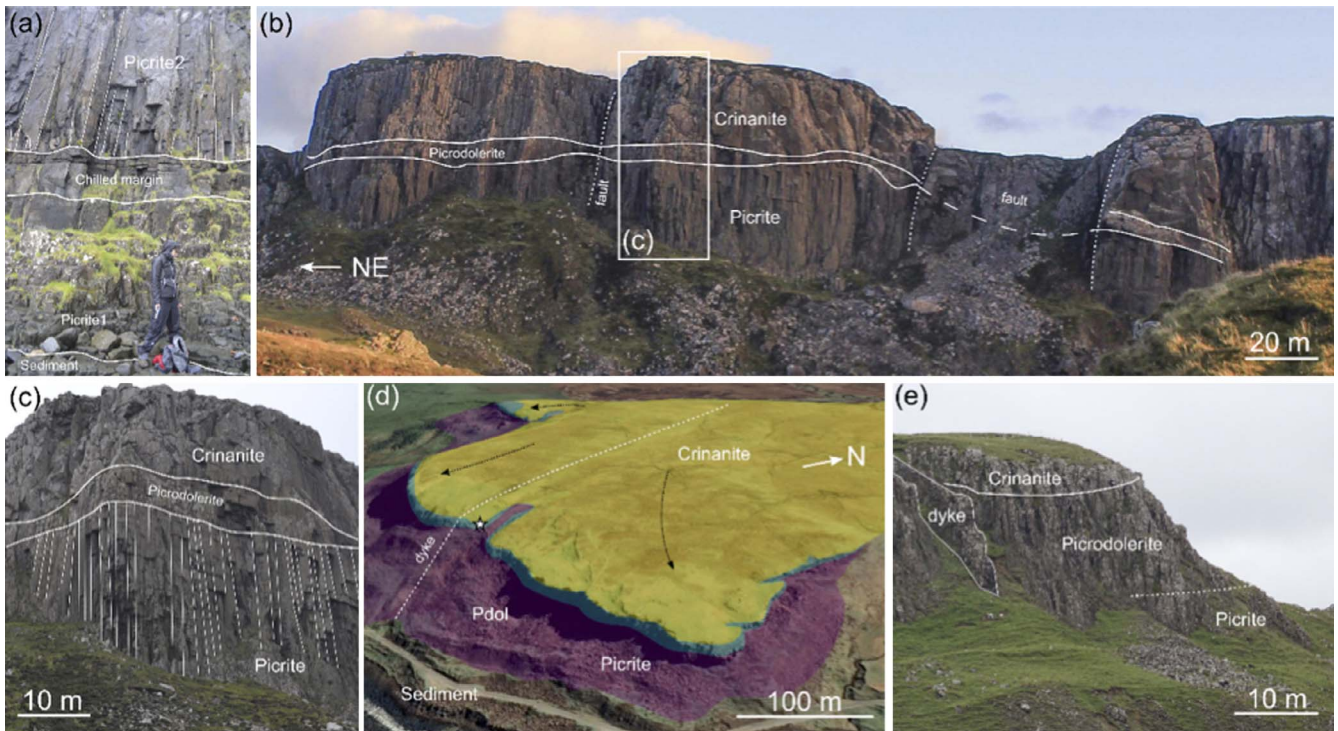
Figure 6. (a–c) The composite, ~115 m thick, Meall Tuath sill. The intrusion is ~115 m thick and comprises an earlier picrodolerite-crinanitic intrusion that was intruded by a later ~40-m-thick picrite. The samples collected near the top of the exposed outcrop are weathered, with no evidence for an upper chilled margin. (a) The later picrite (picrite 2) has well-developed chilled margins against the enclosing picrodolerite-crinanite (labelled picrite 1). (b) The later picrite has columnar jointing (enlarged area shown in (c)), suggestive of significant cooling of the earlier picrodolerite-crinanite before the picrite was intruded. Image courtesy of Geoff Allan. (d, e) The composite Creagan Iar sill. (d) Areal view of the Creagan Iar sill, with false colour superimposed: purple is the early picrite, blue is the picrodolerite base of the later unit and yellow is the overlying crinanite. Black dashed arrows indicate magma transport direction within the composite sill (from Fyfe et al., 2021) and the star marks the location of the sample traverse. 3D image from Google Earth. (e) The contact between the PCU and the underlying earlier picrite (>80 m thick) is not well defined in outcrop, and the presence of columnar jointing through the entire cliff face suggests these two units cooled together.

apparently entirely surrounded by pyroxene grains (Fig. 10c, d), which are either equant and subhedral grains joined on growth faces, or subhedral to anhedral grains that surround larger subhedral olivine grains. The size of the clinopyroxene grains is greater than that in Meall Tuath, and the extent to which they are sintered to, and apparently surround, olivine grains is much greater.

Clustered clinopyroxene grains become larger and volumetrically dominant towards the top of our traverse, commonly entirely surrounding apparently isolated olivine grains (Fig. 10d). The size of individual clinopyroxene grains within these bi-mineralic clusters become larger and more irregular with increasing height, with included plagioclase grains on their margins attesting to some interstitial growth (Fig. 10e), although the proportion of
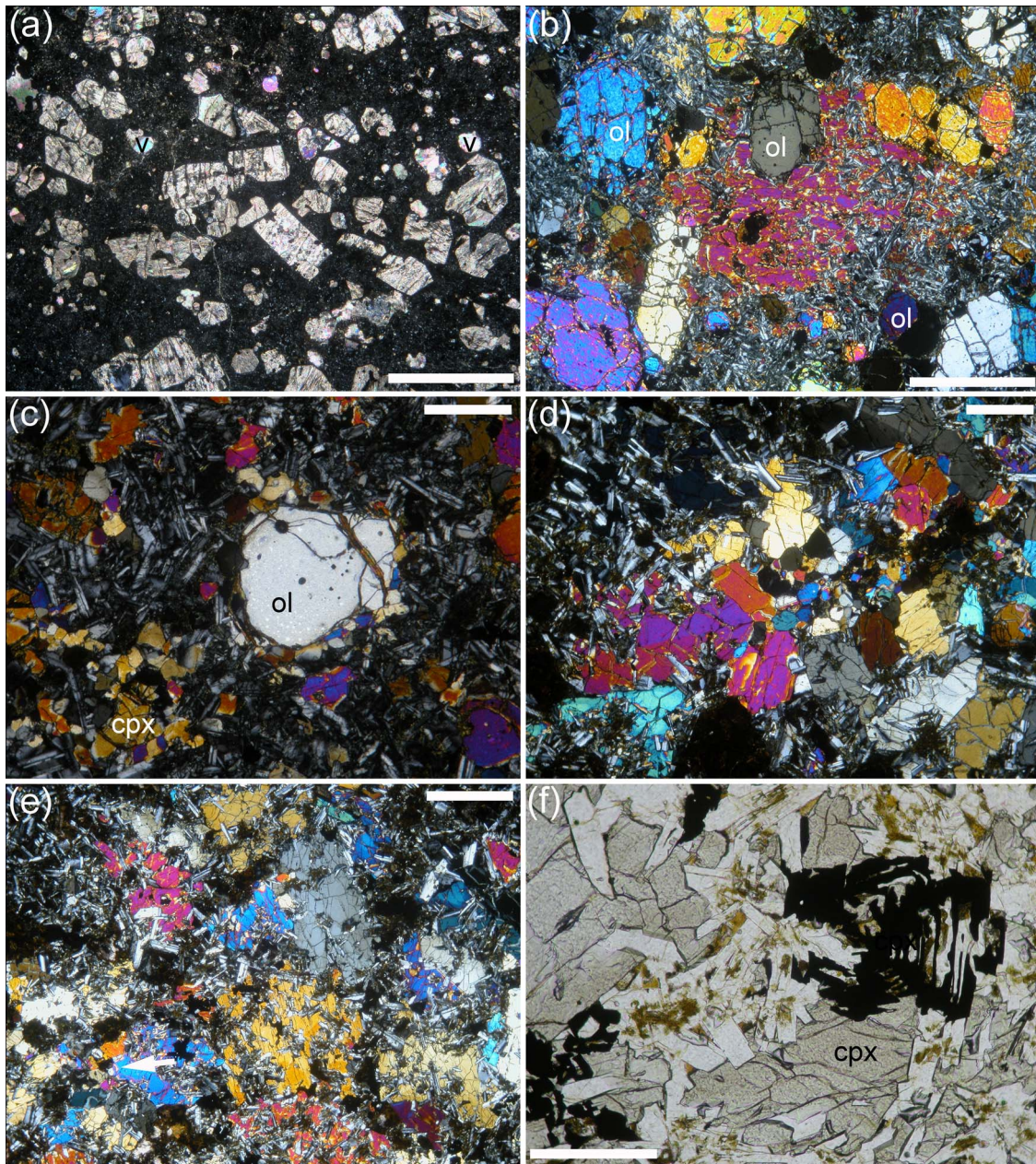
Figure 7. Photomicrographs of the Meall Tuath sill: all images except (f) taken under crossed polarised light. Abbreviations: ol, olivine; cpx, clinopyroxene; v, vesicle; ox, Fe-Ti oxides. (a) Basal chill of the Meall Tuath sill (sample MT01), with almost completely altered olivine crystals forming clusters, with some apparently isolated grains. The rounded bright patches are vesicles, now filled with calcite (two are labelled v). The scale bar is 2 mm long. (b) Sample MT18, collected 5 m from the base of the PCU. Rounded olivine grains (representative examples are labelled) are surrounded by equant, randomly oriented plagioclase grains: both equant phases are enclosed by extensive clinopyroxebe oikocrysts. Scale bar is 2 mm long. (c) Sample MT15, collected 13.3 m from the base of the PCU. An isolated olivine grain, exhibiting some crystal growth faces, is surrounded by small clinopyroxene grains that may have nucleated heterogeneously on its surface. Note the clusters of compact clinopyroxene grains present elsewhere in the field of view (one such is labelled 'cpx'). Scale bar is 0.5 mm long. (d) Sample MT11, collected 23.6 m from the base of the PCU. Clinopyroxene grains form well-sintered clusters. The outermost grains are relatively large, with included plagioclase grains, suggestive of continued growth after incorporation into the mush. Scale bar is 0.5 mm long. (e) Sample MT11, collected 23.6 m from the base of the PCU. Much of the clinopyroxene is formed of large oikocrysts. A small cluster of equant clinopyroxene grains is arrowed. Scale bar is 1 mm long. (f) Sample MT9, collected 29.1 m from the base of the PCU. The Fe-Ti oxide grains are non-compact, with the crystallographic branching indicative of diffusion-limited growth. The highly euhedral nature of these grains attests to their growth in a liquid-rich environment. Scale bar is 0.25 mm long.

inclusion-free clinopyroxene (i.e. pyroxene that did not grow *in situ* within a mush) is always higher than that at equivalent levels in the Meall Tuath sill. When clinopyroxene and olivine are considered together, the average size of clusters of mafic minerals (olivine ± clinopyroxene, and clinopyroxene alone) decreases with increasing height, but at a slower rate than that of the olivine-only clusters (Table 3). This faster upwards decrease in the

average size of olivine-only clusters is due to the separation of individual olivine grains in the bi-mineralic clusters. Note that the difference between the average size of individual olivine grains and the grain clusters (olivine-only below pyroxene-in, and bi-mineralic above pyroxene-in) decreases with height (Fig. 9), associated with a smaller number of individual grains within each cluster.
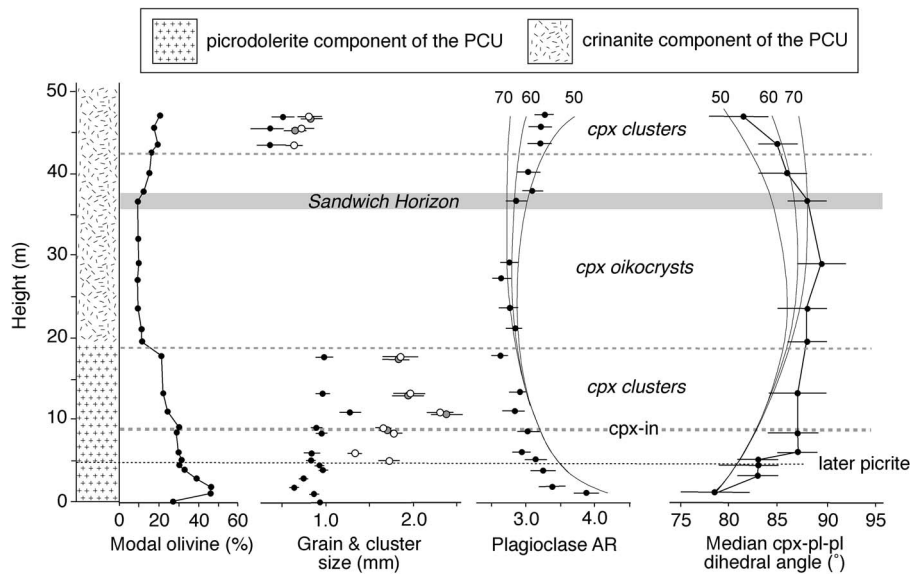
Figure 8. The stratigraphy of the picrodolerite-crinanite component of the composite Meall Tuath sill, together with the variation in olivine mode, olivine grain size, the median value of the clinopyroxene-plagioclase-plagioclase dihedral angle, and the average apparent aspect ratio (AR) of the plagioclase in the PCU. The sandwich horizon is placed where the olivine mode is at a minimum. The position in the stratigraphy where the later picrite intruded is shown as the fine dotted line. The three dashed lines show, in order from the base of the sill, the position of the arrival of equant clinopyroxene, the loss of clusters of equant clinopyroxene and the position of their re-appearance (see text for more details). The olivine grain size data include the average size of individual olivine grains (shown as black dots) and the average size of olivine clusters (white circles). The expected values of dihedral angle and AR are shown by the continuous lines (calculated using the compilations of Holness et al. (2012a) and (2014)) for sill thicknesses of 50 m, 60 m and 70 m.
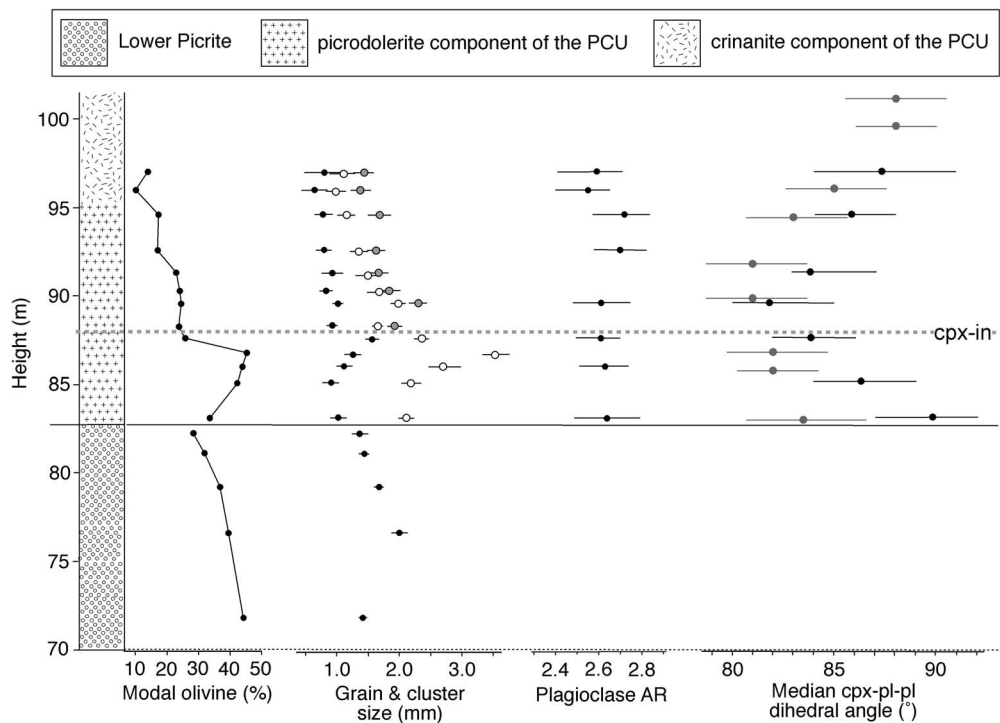
Figure 9. The stratigraphy of the composite sill exposed at Creagan Iar, together with the variation in olivine mode, olivine grain size, the median value of the clinopyroxene-plagioclase-plagioclase dihedral angle, and the average apparent aspect ratio (AR) of the plagioclase. The contact between the two units of the composite body is shown as a heavy dashed line. The average size of individual olivine grains is shown as black dots, whereas that of olivine clusters is shown as white circles. The median dihedral angles from the Shiant Isles Main sill PCU are shown for comparison with those from the Creagan Iar picrodolerite-crinanite, superimposed so that the base of the Shiant PCU corresponds to the contact between the two components of the Creagan Iar sill.

Plagioclase forms randomly oriented tablets throughout the PCU, commonly with well-developed normal zoning, and of similar size to that in the Shiant PCU (Table 3). The skew of the populations of long axes are similar to that reported for sills by Holness et al. (2017b) (Fig. 5). Grain shape, as quantified by AR (and measured for grains that are not enclosed by clinopyroxene), is invariant through our sample traverse (Table 3; Fig. 9).
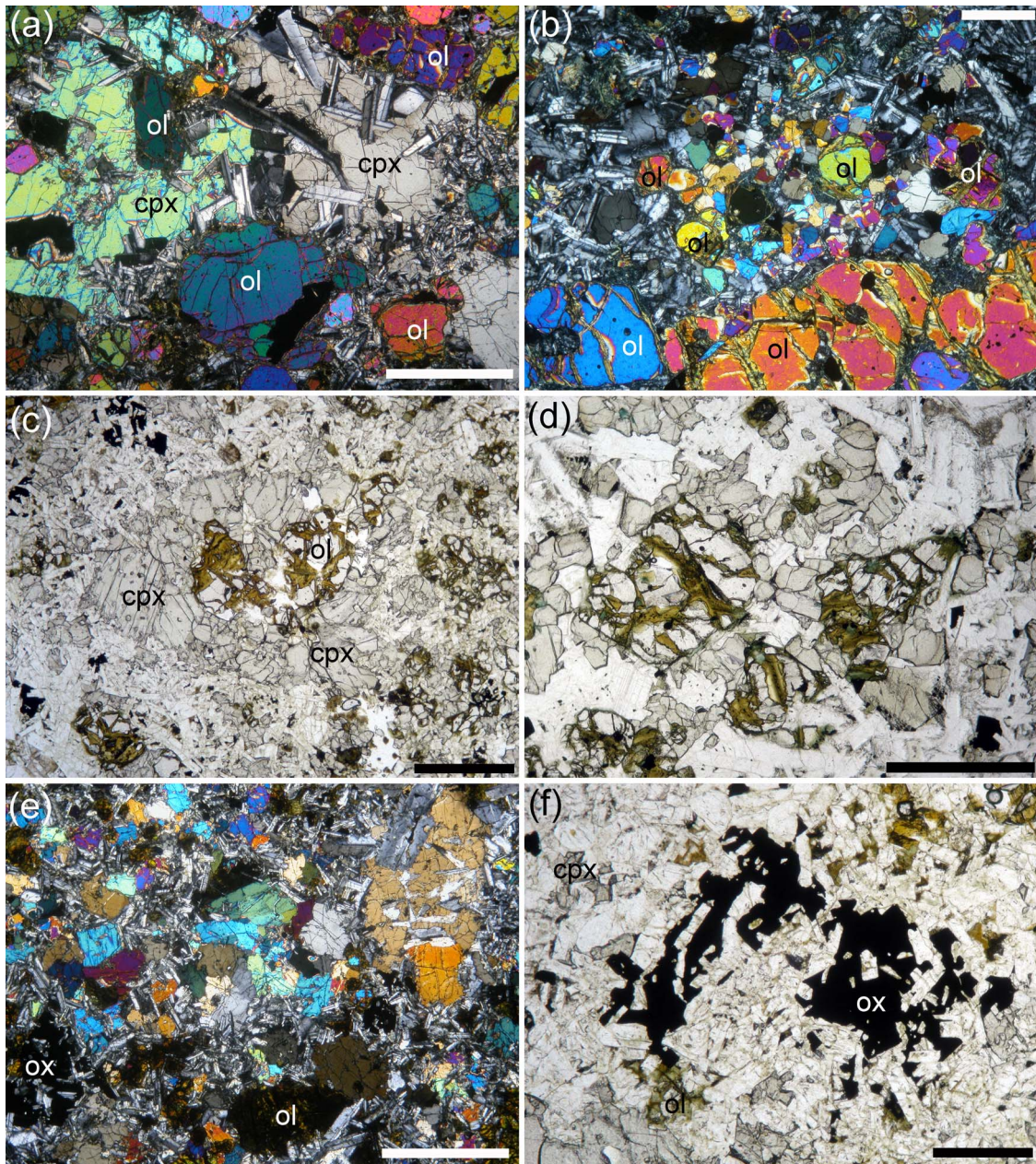
Figure 10. Photomicrographs of the Creagan Iar sill. (a) Sample CI 10, collected from the base of the PCU. Abundant rounded olivine grains and equant plagioclase set in clinopyroxene oikocrysts. Note how the enclosed plagioclase grains are larger than those outside the oikocrysts. Scale bar is 2 mm long. (b) Sample CI 5, collected 6.5 m above the base of the PCU. A polymineralic grain cluster formed of olivine and clinopyroxene. The pyroxene grains are generally smaller than those of olivine. Scale bar is 0.5 mm long. (c) Sample CI 1, collected 11.6 m above the base of the PCU, showing a cluster of three rounded olivine grains (all highly altered), completely surrounded by fresh, equant, grains of clinopyroxene of a similar size to those of the olivine. Scale bar is 1 mm long. (d) Sample CI 3, collected 83 m above the base of the PCU, showing a group of apparently isolated olivine grains (all highly altered) cemented into a coherent cluster by abundant equant grains of clinopyroxene of a similar size to that of the olivine. Scale bar is 1 mm long. (e) Sample CI 18, collected ~14 m above the base of the PCU. The clinopyroxene grains are larger than those in (b) and, although they have inclusion-free equant cores, have irregular overall shapes, with included grains of plagioclase at their margins denoting significant interstitial growth within the mush at their margins. At this level in the sill, olivine grains are generally almost entirely replaced by low-temperature hydrous minerals. Note the interstitial Fe-Ti oxides. Scale bar is 2 mm long. (f) Sample CI 17, collected 13 m above the base of the PCU, showing the interstitial nature of the Fe-Ti oxides, with abundant enclosed and partially enclosed plagioclase grains. Scale bar is 0.5 mm long.

Ilmenite is present as elongate euhedral grains. Magnetite forms large, subhedral to anhedral grains in the lower part of the PCU. With increasing stratigraphic height, they become more euhedral, commonly with the non-compact morphology and crystallographic branching indicative of diffusion-limited growth. In the topmost ~5 m of our traverse, magnetite reverts to being anhedral, forming oikocrysts with abundant inclusions of plagioclase (Fig. 10f). Small quantities of highly altered interstitial analcime are present throughout the traverse.

The median clinopyroxene-plagioclase-plagioclase dihedral angles in the Creagan Iar PCU are also shown in Fig. 9 (values given in Table 3), together with Θ_{cpp} in the lowest 15–20 m of the Shiant Isles PCU for comparison. Dihedral angles in the Creagan Iar PCU display the same pattern of high dihedral angles at the contact with the underlying picrite, decreasing to a minimum

and then increasing again with increasing stratigraphic height. The value of Θ_{cpp} at the contact is considerably higher than that at the base of the Shiant PCU, but the length-scale over which it reverses is the same.

DISCUSSION
Morphological evolution of plagioclase grains during crystallisation

Plagioclase grain shape in the Shiant Isles Main sill crinanite depends on the local volume proportion of plagioclase, in agreement with experimental observations (Pupier et al., 2008; Schiavi et al., 2009). Our data extend the trend observed in experimental charges (Fig. 4), and show a continuous reduction in AR due to impingement as the plagioclase mode increases. In detail, however, it is unlikely that our data form a true extension of the experimental results, since the cooling rate of the Shiant crinanite was significantly lower than that of the experiments, meaning that plagioclase was always likely to have been more equant in the former. While the trajectory of a crystallising magma on the plot of AR vs % solidified will have a negative slope, flattening to the final value in the (almost) fully solidified basalt/dolerite, the position of that trajectory will be shifted to higher AR as the cooling rate increases.

The greater values, and range of values, of AR observed in the Shiant crinanite near the sandwich horizon at ~120 m stratigraphic height (Fig. 2) are consistent with the compositional evolution of the magma documented by Gibb & Henderson (1996, 2006). It can be explained by the progressively earlier nucleation and growth of clinopyroxene in the fractionating magma, preserving progressively earlier stages of plagioclase cluster development typified by open and loose frameworks in which the original higher ARs have not been significantly reduced by post-impingement growth.

A generally higher apparent AR of plagioclase grains within oikocrysts compared with those outside was also noted by Mathison (1987), who attributed it to higher undercoolings during the early phase of growth. Although he did not provide data relating plagioclase shape to the volumetric proportion enclosed by pyroxene, his observations can be explained by our hypothesis that AR decreases during solidification due to the effects of impingement.

The values of Θ_{cpp} in the upper part of the Shiant crinanite are lower than expected from a comparison of the data compilation of Holness et al. (2012a) (Fig. 2). We do not consider it likely that this part of the composite sill cooled more rapidly than the equivalent region of a single-component sill intruded into cold country rock (c.f. Holness et al., 2012a). Instead, it is possible that the low recorded angles are an artefact of our choice to confine measurement to regions outside the oikocrysts, thus biasing our measurements towards lower values (c.f. Holness et al., 2005).

Our results emphasise the importance of minimising the compositional range of suites of mafic rocks used for comparative studies of plagioclase grain shape, to ensure that the final shape in the fully solidified rock is subject only to variations in cooling rate and not to the timing of impingement caused by differences in liquid composition. Our results also suggest that while the relationship between AR and cooling rate determined by Holness (2014) is valid for the groundmass of a porphyritic rock, AR should not be used to deduce crystallisation times for the phenocrysts unless it can be demonstrated that they have been released from disaggregated, almost completely solidified, crystal mushes in which impingement played a significant role in determining their final shape. Further work is needed to quantify the morphology of grains grown in isolation as a function of temperature and cooling rate.

Intrusion sequence in the Trotternish composite sills

While the relative timing of the two components of the composite Meall Tuath sill is straightforwardly established by the well-developed chilled margins of the later picrite, the relative timing of the two components of the Creagan Iar sill cannot be determined in outcrop. Schofield (2009) argues, on the basis of a correlation with sills of the central dolerites exposed on the east coast of the Trotternish Peninsula, that the Creagan Iar picrite post-dated the associated PCU, but we argue below that our microstructural data demonstrate that the picrite was the earlier of the two.

Critically, the stratigraphic distribution of olivine in the exposed part of the Creagan Iar PCU (Fig. 9) is similar to that seen at the base of S-type bodies (Marsh, 1988). This unit must therefore be exposed close to, or at, its base at Creagan Iar. This is consistent with the observation that the top of the picrite is close to the base of the overlying picrodolerite-crinanite at nearby Osmigarry (Fig. 1), where these two components are separated by a thin screen of Jurassic sediments (Gibson & Jones, 1991). However, the lower part of the Creagan Iar PCU does not have the relatively fine grain size that might be expected if the magma intruded into a cold environment, highly suggestive of the PCU post-dating the picrite.

The microstructures of the Creagan Iar PCU provide further evidence of this revised relative timing. The intrusion of the second of the two units almost certainly took place when the first was completely, or almost completely, solidified: if the PCU were the earlier of the two, we would expect a monotonic decrease in Θ_{cpp} towards its base, in a similar manner to that observed for Meall Tuath (Fig. 8). Although there can have been no sub-solidus textural equilibration at the contact due to heating by the later 83-m-thick picrite (since, in comparison, the 50-m-thick picrite at Meall Tuath caused no measurable subsolidus textural equilibration in the associated earlier picrodolerite), there is a substantial reversal in Θ_{cpp} at the base of the Creagan Iar PCU on the same length scale as that observed at the base of the Shiant Isles PCU (Figs 2 and 9). From a comparison with the Shiant Isles PCU, for which the earlier age of the underlying picrite is unequivocal (Gibb & Henderson, 1996), the high values of Θ_{cpp} in the lower 7 m of the Creagan Iar PCU must have been a consequence of slow solidification rather than a later, sub-solidus, textural equilibration. The Creagan Iar PCU thus post-dates the underlying picrite. Both the mode and the average grain size of olivine in this underlying picrite decrease towards the contact with the overlying PCU, suggestive that the PCU intruded close to its upper margin, in a similar fashion to the Shiant Isles PCU, which intruded the earlier picrite only a few metres from its roof (Fig. 2).

The thickness of the Trotternish sills

Although the thickness of the Shiant Isles Main Sill is tightly constrained (Gibb & Henderson, 1984, 1996), that for the Meall Tuath and Creagan Iar sills is not. However, Θ_{cpp} and AR can be used to estimate thickness, since these parameters are controlled by cooling rate. The values of both parameters in the upper reaches of the Meall Tuath PCU are consistent with an overall thickness of 50–60 m (Fig. 8), suggesting that <10 m has been lost

to erosion, in agreement with Schofield (2009). However, the lower-than-expected AR and higher-than-expected Θ_{cpp} in the lower part of the Meall Tuath PCU suggest slower-than-expected cooling rates in this part of the intrusion. This lower cooling rate cannot be a result of heating by the later picrite, as there is no evidence of sub-solidus recrystallisation. These departures from the expected values for a simple, closed-system, non-fractionating body must be caused by processes occurring early in the intrusion's history. The absence of a marginal reversal in AR, which is present in all the sills examined by Holness et al. (2017b), is significant in this regard. In a forthcoming contribution, we argue that the absence of a marginal reversal is indicative of sustained magma flow past the location of the sample traverse, which must therefore represent part of a conduit feeding magma either to the surface or to distant parts of the same intrusion, during a prolonged intrusion event. It is therefore possible that this long-lived flow heated the country rock sufficiently to result in slower cooling than assumed for the calculated values of AR and Θ_{cpp}.

The thickness of the Creagan Iar PCU is less easy to establish. The dihedral angles in our traverse are consistently higher than those in the Shiant Isles PCU (albeit with overlapping 2σ uncertainties; Fig. 9), with correspondingly lower AR (~2.6 instead of ~2.8), suggestive of a slower cooling of the Creagan Iar PCU. Both units form part of composite bodies, so the cooling rate is dependent on the relative size and timing of the component intrusions. The Creagan Iar PCU overlies an older 83-m-thick picrite sill, much thicker than the 25 m of the early picrite of the Shiant Isles Main sill, with potentially greater thermal effects. The Creagan Iar PCU is thus likely to be thinner than the Shiant PCU. If the amount of olivine crystal cargo were similar to that in the closely related Meall Tuath PCU, we might perhaps expect a similar fraction of the Creagan Iar PCU to be picrodolerite, giving an overall thickness of 33–40 m. The same argument, using the thickness of the Shiant picrodolerite instead, suggests an overall thickness of 30 m for Creagan Iar. We may therefore be missing 25 m, at most, of the top of the PCU.

Post-emplacement fractionation

The Shiant Isles Main Sill was filled by magma that carried a cargo comprising olivine, plagioclase (Gibb & Henderson, 1996) and chrome spinel (Holness et al., 2017a), whereas the magma that formed the two Trotternish sills appears to have carried only olivine and chrome spinel. Furthermore, clinopyroxene is entirely poikilitic in the Shiant, but locally forms clusters of compact grains in the two Trotternish sills. These minor compositional differences are consistent with their wide geographic separation and different feeder systems (Fyfe et al., 2021).

A similar pyroxene morphological variation to that described in the two Trotternish sills is present in the Holyoke and Cohasset flood basalts, with pyroxene oikocrysts in the entablature while the colonnade is typified by clusters of granular equant grains. This difference is attributed by Philpotts & Dickson (2000) and Philpotts & Philpotts (2005) to recrystallisation of original poikilitic grains in the slower-cooled colonnade, but we argue that the analogous morphological transition to clusters of equant, compact, pyroxene observed in the Trotternish sills is a consequence of fractionation, leading to abundant nucleation of pyroxene in the bulk magma followed by cluster formation by synneusis during convection.

The Meall Tuath PCU displays a step-wise increase in Θ_{cpp} at ~6 m height (Fig. 8): this is associated with a poorly defined step-wise decrease in AR, with approximately constant values of these two parameters up to the sandwich horizon. Such step-wise

changes are observed in fractionating systems and are caused by the addition of a phase to the liquidus assemblage, which slows the cooling rate by increasing the contribution of latent heat to the enthalpy budget (Holness et al., 2007; Morse, 2011). The thickness of the floor mush in the Meall Tuath sill can therefore be constrained to 2.5–4 m by the off-set between this step change and the first appearance of the compact, equant, clinopyroxene in the stratigraphy (c.f. Holness et al., 2017c).

Step-wise changes in Θ_{cpp}, associated with the appearance of new liquidus phases, are not observed in either the Creagan Iar or the Shiant Isles PCU, despite the evidence for fractionation-driven saturation of the Creagan Iar bulk magma in clinopyroxene and evidence of fractionation of the Shiant magma presented by Gibb & Henderson (1996, 2006) and Henderson et al. (2000). The absence of a clinopyroxene-in Θ_{cpp} step in Creagan Iar is perhaps a consequence of the larger effect of the underlying earlier picrite, which significantly slowed the solidification rate of the basal 5–6 m, masking any effects of fractionation. That the saturation of the magma in Fe-Ti oxides recorded by the morphological change at ~80 m (Fig. 3) is not associated with a step-wise increase in Θ_{cpp} in the Shiant PCU is perhaps due to insufficient sample spacing coupled with the small magnitude of the oxide-in dihedral angle step (e.g. Holness et al., 2007).

Convection during solidification of the Trotternish sills
Evidence provided by plagioclase

The relatively constant values of AR through the central part of the Meall Tuath sill might be used to argue that a significant part of the plagioclase growth history involved suspension of individual grains in a convecting magma (Fig. 8). However, AR is strongly negatively correlated with Θ_{cpp} (Fig. 11): that microstructural speedometers recording both the early and late stages of solidification correlate so strongly shows that plagioclase grain growth was predominantly *in situ*. In contrast, plagioclase shape in both the Shiant Isles (considering only that outside the pyroxene oikocrysts) and Creagan Iar PCUs is stratigraphically invariant, with no correlation with Θ_{cpp} (Fig. 11). Such spatial invariance of shape, caused by plagioclase growth predominantly at the same cooling rate regardless of its final position, can only be achieved if grains spent a significant part of their growth history suspended in a convecting magma before accumulating on the floor (Holness et al., 2017b), in agreement with Holness et al. (2017a) who concluded, from an analysis of olivine grain size, that the Shiant magma underwent vigorous convection. The evidence of extensive frameworks of plagioclase preserved by the oikocrysts in the Shiant suggests that abundant clustering of plagioclase took place before settling (c.f. Philpotts et al., 1998, 1999; Philpotts & Dickson, 2000).

An exception to the general spatial invariance of AR in the Shiant PCU occurs in the basal 10–15 m, in which it decreases downwards. This decrease coincides not only with the basal fining-upwards sequence formed by the early settling of almost all the olivine cargo (Holness et al., 2017a), but also the point at which Θ_{cpp} undergoes its marginal reversal towards higher-than-expected values (Fig. 2). We suggest that AR in this basal 10 m is recording some nucleation and growth of plagioclase *in situ* in the pore spaces of the crystal mush formed by the rapid settling of the incoming olivine cargo: the upwards increase in AR (and hence increasing cooling rate) may be due to the decreasing influence on the cooling rate of the underlying earlier picrite, as evident in the associated decrease in Θ_{cpp}. A further factor may perhaps be an upwards-increasing contribution of plagioclase
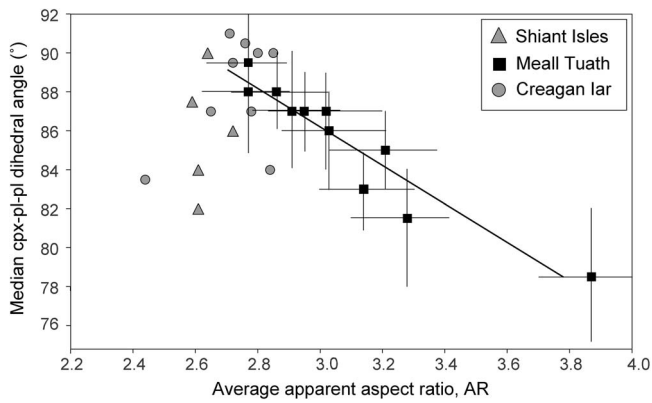
Figure 11. The variation of average apparent aspect ratio (AR) of plagioclase with the median clinopyroxene-plagioclase-plagioclase dihedral angle, Θ_{cpp}, for the Shiant Isles Main sill PCU and the Meall Tuath and Creagan Iar sills. The uncertainties are shown only for the Meall Tuath dataset, for clarity. The best fit straight line through the latter has $R^2 = 0.896$.

grown predominantly as suspended grains, which then settle to the floor.

The plagioclase grain size in both the Creagan Iar and the Shiant Isles PCU is coarser than that in the Meall Tuath sill (Tables 1–3). Although a coarser grain size has been argued to be indicative of systems undergoing vigorous convection (Holness et al., 2017b), the grain size in all three sills is comparable to that seen in sills in which AR varies with height (Holness et al., 2017b) and is significantly smaller than that found in dykes of the same width in which AR is invariant (in which, for comparison, the average grain size is of the order 1 mm, Holness et al., 2017b). Additionally, the skew of the populations of plagioclase long axes is similar to that of the sills investigated by Holness et al. (2017b), rather than the lower skew found in dykes (Fig. 5).

Holness et al. (2017b) argued that the differences in grain size between sills and dykes of comparable thickness are attributable to the absence of convection in sills compared to the vigorous convection in dykes, with the narrower range of grain size in dykes attributable to the high mobility of the suspended grains, with loss of the very largest by flotation or settling and loss of the smallest by the rapid Ostwald ripening driven by the temperature fluctuations experienced by suspended grains in a convecting system (e.g. Mills et al., 2011). That we find a relatively fine grain size and high skew in all three sills regardless of whether there is strong evidence for plagioclase growing while suspended in vigorously convecting magma (e.g. the Shiant Isles Main sill PCU and the Creagan Iar PCU) or evidence for *in situ* grain growth in marginal solidification fronts (e.g. the Meall Tuath sill) suggests that the explanation of Holness et al. (2017b) is too simplistic. The finer plagioclase grain sizes in both the Shiant and the Creagan Iar PCUs compared to those in similar-sized dykes may be a consequence of their poikilitic microstructure. While oikocrysts are commonly interpreted as a consequence of interstitial growth under conditions of limited nucleation, Barnes et al. (2016) suggest that at least the central parts of oikocrysts may form in the bulk magma before settling to the floor: an early formation of plagioclase clusters that are cemented by heterogeneously nucleated pyroxene while suspended in convecting magma would result in a generally finer plagioclase grain size compared to grains grown in isolation. This hypothesis should be tested by examining the grain size of plagioclase in non-poikilitic basaltic sills that show invariant AR.

Evidence provided by olivine and clinopyroxene

In the Meall Tuath PCU, the olivine mode decreases from 46 to ~30 vol% in the lowermost few metres, associated with fining upwards (Fig. 8). Comparison with the Shiant Isles PCU suggests this records the settling of most of the olivine crystal cargo onto an inwards-propagating surface created by the *in situ* nucleation and growth of plagioclase (as demonstrated by the stratigraphic variation of AR). Further comparison with Shiant suggests that the magma in the Meall Tuath PCU then underwent a period of convection. Although the original cargo contained extensive clusters of olivine, that such clusters contain compact grains of clinopyroxene only above ~8 m height (Fig. 7c, d) means that clusters must have either formed *ab initio* post-emplacement, or be the products of enlargement of originally small clusters from the cargo, with settling hindered by convection. The poorly defined fining-upwards of clusters above ~10 m suggests that the convective strength then progressively waned. Importantly, the size of the few olivine primocrysts and clusters preserved in the uppermost exposed reaches of the Meall Tuath PCU are smaller even than the smallest grain size distributions at the floor, instead of matching that of the coarsest grains at the floor, as seen in the Shiant (Holness et al., 2017a). There were no convection currents sufficiently strong to carry large olivine clusters up to the roof during the period in which the largest clusters were accumulating at the floor.

There are no clusters of olivine primocrysts above ~18 m—that this was a consequence of convection becoming too weak to keep mafic particles suspended is demonstrated not only by the abruptness of the drop in olivine mode (Fig. 7), but also because clinopyroxene also changes habit to interstitial. Above this height in the sill, convection had weakened to the point that newly formed olivine and clinopyroxene grains could not be kept suspended, so all growth of these phases took place at the magma-mush interface. The constant olivine mode of <10 vol% is that which grew from the bulk liquid.

This picture of relatively static magma immediately post-emplacement, permitting rapid settling, followed by a period of (weak) convection is supported by a consideration of the relative rates of solidification and settling in a static magma. If we assume a density contrast of 700 kg m^{-3} and a liquid viscosity of 3.9–8.5 Pa s (following Holness et al., 2017a), the settling velocity of the average 0.7-mm-diameter grains in the lower 2 m of the Meall Tuath picrodolerite is 2.5×10^{-5}–5×10^{-5} m s^{-1}, requiring ~10 days to settle 30 m. The simple thermal model of Holness et al. (2012a), based on conductive cooling into country rock initially at 0°C, a crystallisation interval of 1200–1000°C, and a sill thickness of 50–70 m, tells us that the sill floor would have been completely solidified to a height of 2 m within ~100 days. Given the simplicity of the thermal model (justified, we argue, because we know too little about the actual thermal conditions during sill emplacement and inflation to create a more sophisticated model), and the fact that we only need to form a mushy layer sufficient to support settled olivine grains at this height, rather than attain complete solidification, the correspondence of these timescales is reassuring: much of the olivine cargo could have sunk to the floor during the earliest stages of solidification. However, the presence of bi-mineralic clusters of >2 mm average diameter almost 20 m above the sill base indicates an imbalance between timescales of settling and solidification of three orders of magnitude. This imbalance was attributed by Gibb & Henderson (1992) to hindered settling caused by high particle concentrations or the presence of gas bubbles, but we argue that the evidence provided by clusters of clinopyroxene points to the action of convective currents that

kept dense clusters of olivine and pyroxene suspended for the ~15 years required for the floor solidification front to reach ~18 m height.

Importantly, while the microstructures and the stratigraphic distribution of olivine and pyroxene provide evidence of convection during the early stages of solidification, despite being more buoyant than either olivine or pyroxene, plagioclase shape in the Meall Tuath sill suggests growth predominantly *in situ*. We suggest this difference lies in the location of nucleation. Olivine was brought into the sill as cargo, with abundant tiny grains remaining in suspension after the initial period of settling, and equant clinopyroxene grains nucleated heterogeneously on the surfaces of suspended olivine grains—the apparently olivine-free pyroxene clusters (e.g. Fig. 7c, d) may have an olivine grain out of the plane of section, or the pyroxene nucleated on particles of something else in the bulk magma. In contrast, the stratigraphic variation of plagioclase AR points to nucleation at the magma-mush interface aided, at least in the early stages, by a cold floor. This suggests that the shape-invariant plagioclase observed in many dykes, as well as in both Shiant and Creagan Iar, requires more vigorous convection than that in the Meall Tuath sill to ensure plagioclase grains are entrained from their marginal nucleation sites.

The morphology of olivine and pyroxene grains in Creagan Iar also supports convection: we see the same transition from interstitial to compact and equant clinopyroxene grains as in Meall Tuath, and pyroxene incorporation into olivine clusters indicative of suspension in a fractionating convecting magma. This signature of convection persists through our incomplete traverse of the Creagan Iar PCU. In contrast to both Shiant and Meall Tuath, however, the crystal mush at the basal contact of the Creagan Iar PCU was created by the settling not only of olivine (and, later, clinopyroxene) but also of plagioclase. The uniform values of AR demonstrate there was little, or no, *in situ* nucleation and growth of plagioclase even at the basal contact. This difference must be due to the relatively high temperature of the floor of the PCU in this composite sill, as suggested by the higher values of Θ_{cpp} compared to those at the base of the Shiant PCU (Fig. 9).

In contrast to the Meall Tuath and Shiant PCUs, there is no basal fining-upwards sequence in Creagan Iar. Additionally, above ~87 m stratigraphic height, three abrupt changes are seen: the olivine mode halves (followed by a slow decrease towards values expected for the carrier liquid only); the size of individual olivine grains and clusters (both olivine-only and bi-mineralic) decreases, with a subsequent further fining upwards; and the values of Θ_{cpp} start to increase upwards, as expected for a single component body (Fig. 9). These observations can be accounted for if convection was sufficiently vigorous that settling was delayed, resulting in the coarsening of both individual grains and clusters. The cargo had mostly settled (together with some plagioclase grown as suspended grains) by the time the top of the solidification front had reached ~87 m, causing the abrupt decrease in olivine mode. The olivine primocrysts found above this level were formed either by growth of the very small olivine cargo crystals still remaining in the bulk magma, or by post-emplacement nucleation and growth in the bulk magma. Interestingly, the olivine grain size is relatively small and essentially invariant above ~87 m, suggesting that grains were rapidly incorporated into clusters, precluding further growth as isolated grains. The fining-upwards of clusters is in contrast to the coarsening-upwards in the Shiant Isles PCU but, in common with Meall Tuath, we suggest it is recording progressively waning convective strength.

The change in magnetite habit, from dendritic to interstitial, in the topmost ~5 m of our traverse (Fig. 10f) is similar to changes in habit of olivine and clinopyroxene in the Meall Tuath PCU, further suggesting that convective vigour in the Creagan Iar sill had become insufficient to maintain magnetite grains in suspension, with growth subsequently confined to the solidification front. However, the magnetite in Meall Tuath is commonly of hopper/dendritic habit throughout the sill, so the change in magnetite habit in the Creagan Iar is perhaps not significant.

CONCLUSIONS

The microstructural variation in the three sills examined here can only be accounted for if the magma convected for some time after emplacement. The stratigraphic variation of plagioclase grain shape and the size and composition of grain clusters points to vigorous and long-lived convection during solidification of the Shiant Isles Main sill PCU, vigorous but perhaps short-lived convection in the Creagan Iar PCU, and weak and short-lived convection in the Meall Tuath sill.

The evidence for convection preserved by the mafic phases in the Meall Tuath sill is in contrast to the variation of plagioclase shape indicative of *in situ* growth at the margins. The absence of the expected stratigraphic shape invariance for this relatively buoyant mineral is most likely due to a difference in the location of nucleation of the different phases, with plagioclase perhaps predominantly nucleating heterogeneously on the floor. If this preference for *in situ* heterogeneous nucleation of plagioclase is general, a stratigraphic shape invariance may indicate convection sufficiently vigorous to entrain plagioclase grains from the marginal mush zones.

The magma in all three sills fractionated during solidification, permitting convection driven by the instability of an upper thermal boundary layer. However, both the Shiant Isles Main sill PCU and the Creagan Iar PCU were emplaced above an earlier, still hot, intrusion, as shown by the continuation of columnar jointing through the contact, the absence of chilled margins, evidence for efficient settling of much of the cargo and high values of Θ_{cpp}. The cooling of both the Creagan Iar and the Shiant PCU was thus highly asymmetric, and we argue that it was this asymmetry of heat flow that enabled the relative longevity of vigorous convection in these two bodies.

DATA AVAILABILITY

The data on which this article is based are available in the article and in its online supplementary material.

References

Applegarth, L. J., Tuffen, H., James, M. R., Pinkerton, H. & Cashman, K. V. (2013). Direct observations of degassing-induced crystallization in basalts. *Geology* **41**, 243–246. https://doi.org/10.1130/G33641.1.

Barnes, S. J., Mole, D. R., Le Vaillant, M., Campbell, M. J., Verrall, M. R., Roberts, M. P. & Evans, N. J. (2016). Poikilitic textures, heteradcumulates and zoned orthopyroxenes in the Ntaka Ultramafic Complex, Tanzania: implications for crystallisation mechanisms of oikocrysts. *Journal of Petrology* **57**, 1171–1198. https://doi.org/10.1093/petrology/egw036.

Bea, F. (2010). Crystallisation dynamics of granite magma chambers in the absence of regional stress: multiphysics modeling with natural examples. *Journal of Petrology* **51**, 1541–1569. https://doi.org/10.1093/petrology/egq028.

Berganz, G. W. & Ni, J. (1999). A numerical study of sedimentation by dripping instabilities in viscous fluids. *International Journal of Multiphase Flow* **25**, 307–320. https://doi.org/10.1016/S0301-9322(98)00050-0.

Boorman, S., Boudreau, A. & Kruger, F. J. (2004). The lower zone–critical zone transition of the bushveld complex: a quantitative textural study. *Journal of Petrology* **45**, 1209–1235. https://doi.org/10.1093/petrology/egh011.

Brandeis, G. & Marsh, B. D. (1989). The convective liquidus in a solidifying magma chamber: a fluid dynamic investigation. *Nature* **339**, 613–616. https://doi.org/10.1038/339613a0.

Brandeis, G. & Marsh, B. D. (1990). Transient magmatic convection prolonged by solidification. *Geophysical Research Letters* **17**, 1125–1128. https://doi.org/10.1029/GL017i008p01125.

Brown, G. M. (1956). The layered ultrabasic rocks of Rhum, Inner Hebrides. *Philosophical Transactions of the Royal Society of London, B* **240**, 1–53. https://doi.org/10.1098/rstb.1956.0011.

Cabane, H., Laporte, D. & Provost, A. (2005). An experimental study of Ostwald ripening of olivine and plagioclase in a silicate melts: implications for the growth and size of crystals in magmas. *Contributions to Mineralogy and Petrology* **150**, 37–53. https://doi.org/10.1007/s00410-005-0002-2.

Coish, R. A. & Taylor, L. A. (1979). The effects of cooling rate on texture and pyroxene chemistry in DSDP Leg 34 basalt: a microprobe study. *Earth and Planetary Science Letters* **42**, 389–398. https://doi.org/10.1016/0012-821X(79)90048-7.

Duchêne, S., Pupier, E., De Veslud, C. & Toplis, M. J. (2008). A 3D reconstruction of plagioclase crystals in a synthetic basalt. *American Mineralogist* **93**, 893–901. https://doi.org/10.2138/am.2008.2679.

Dyck, B. & Holness, M. (2021). Microstructural evidence for convection in high-silica granite. *Geology* **55**, 295–299.

Farr, R. S., Honour, V. C. & Holness, M. B. (2017). Mean grain diameters from thin sections: matching the average to the problem. *Mineralogical Magazine* **81**, 515–530. https://doi.org/10.1180/minmag.2016.080.107.

Foland, K. A., Gibb, F. G. F. & Henderson, C. M. B. (2000). Patterns of Nd and Sr isotopic ratios produced by magmatic and post-magmatic processes in the Shiant Isles Main Sill, Scotland. *Contributions to Mineralogy and Petrology* **139**, 655–671. https://doi.org/10.1007/s004100000169.

Fyfe, J. A., Long, D. & Evans, D. (1993) United Kingdom Offshore Regional Report: the Geology of the Malin–Hebrides Sea Area. HMSO for the British Geological Survey.

Fyfe, L.-J. C., Schofield, N., Holford, S. P., Jerram, D. A. & Hartley, A. (2021). Emplacement of the Little Minch Sill Complex, Sea of Hebrides Basin, NW Scotland. *Journal of the Geological Society* **178**, 3, jgs2020-177. https://doi.org/10.1144/jgs2020-177.

Gibb, F. G. F. & Gibson, S. A. (1989). The Little Minch Sill Complex. *Scottish Journal of Geology* **25**, 367–370. https://doi.org/10.1144/sjg25030367.

Gibb, F. G. F. & Henderson, C. M. B. (1984). The structure of the Shiant Isles Sill Complex, Outer Hebrides. *Scottish Journal of Geology* **20**, 21–29. https://doi.org/10.1144/sjg20010021.

Gibb, F. G. F. & Henderson, C. M. B. (1992). Convection and crystal settling in sills. *Contributions to Mineralogy and Petrology* **109**, 538–545. https://doi.org/10.1007/BF00306555.

Gibb, F. G. F. & Henderson, C. M. B. (1996). The Shiant Isles Main Sill: structure and mineral fractionation trends. *Mineralogical Magazine* **60**, 67–97. https://doi.org/10.1180/minmag.1996.060.398.06.

Gibb, F. G. F. & Henderson, C. M. B. (2006). Chemistry of the Shiant Isles Main Sill, NW Scotland, and wider implications for the petrogenesis of mafic sills. *Journal of Petrology* **47**, 191–230. https://doi.org/10.1093/petrology/egi072.

Gibb, F. G. F. & Henderson, C. M. B. (2014). Comments on 'Mafic-ultramafic sills: new insights from M- and S-shaped mineral and whole-rock compositional profiles' by V. Egorova and R. Latypov (J. Petrology, 54: 2155–2191, 2013). *Journal of Petrology* **55**, 1011–1013. https://doi.org/10.1093/petrology/egu015.

Gibson, S. A. (1988) *The geochemistry, mineralogy and petrology of the Trotternish Sill Complex, northern Skye, Scotland*. Unpublished Ph.D. thesis,. Kingston Polytechnic.

Gibson, S. A. & Jones, A. P. (1991). Igneous stratigraphy and internal structure of the Little Minch Sill Complex. Trotternish Peninsula, northern Skye. *Scotland. Geological Magazine* **128**, 51–66. https://doi.org/10.1017/S0016756800018045.

Hammer, J. E. & Rutherford, M. J. (2002). An experimental study of the kinetics of decompression-induced crystallisation in silicic melt. *Journal of Geophysical Research* **107**, ECV 8-1–ECV 8-24. https://doi.org/10.1029/2001JB000281.

Henderson, C. M. B., Gibb, F. G. F. & Foland, K. A. (2000). Mineral fractionation and pre- and post-emplacement processes in the uppermost part of the Shiant Isles Main Sill. *Mineralogical Magazine* **64**, 779–790. https://doi.org/10.1180/002646100549706.

Hersum, T., Hilpert, M. & Marsh, B. (2005). Permeability and melt flow in simulated and natural partially molten basaltic systems. *Earth and Planetary Science Letters* **237**, 798–814. https://doi.org/10.1016/j.epsl.2005.07.008.

Higgins, M. D. (1994). Numerical modelling of crystal shapes in thin sections: estimation of crystal habit and true size. *American Mineralogist* **79**, 113–119.

Higgins, M. D. (1998). Origin of anorthosite by textural coarsening: quantitative measurements of a natural sequence of textural development. *Journal of Petrology* **39**, 1307–1323. https://doi.org/10.1093/petroj/39.7.1307.

Holness, M. B. (2014). The effect of crystallization time on plagioclase grain shape in dolerites. *Contributions to Mineralogy and Petrology* **168**, 1076. https://doi.org/10.1007/s00410-014-1076-5.

Holness, M. B. (2015). Plagioclase growth rates control three-grain junction geometry in dolerites and gabbros. *Journal of Petrology* **56**, 2117–2144. https://doi.org/10.1093/petrology/egv065.

Holness, M. B., Cheadle, M. J. & McKenzie, D. (2005). On the use of changes in dihedral angle to decode late-stage textural evolution in cumulates. *Journal of Petrology* **46**, 1565–1583. https://doi.org/10.1093/petrology/egi026.

Holness, M. B., Tegner, C., Nielsen, T. F. D, Stripp, G. & Morse, S. A. (2007). A textural record of solidification and cooling in the Skaergaard Intrusion, East Greenland. *Journal of Petrology* **48**, 2359–2377. https://doi.org/10.1093/petrology/egm064.

Holness, M. B., Richardson, C. & Helz, R. T. (2012a). Disequilibrium dihedral angles in dolerite sills: a new proxy for cooling rate. *Geology* **40**, 795–798. https://doi.org/10.1130/G33119.1.

Holness, M. B., Humphreys, M. C. S., Sides, R., Helz, R. T. & Tegner, C. (2012b). Toward an understanding of disequilibrium dihedral angles in mafic rocks. *Journal of Geophysical Research* **117**, B06207. https://doi.org/10.1029/2011JB008902.

Holness, M. B., Farr, R. & Neufeld, J. A. (2017a). Crystal settling and convection in the Shiant Isles Main Sill. *Contributions to Mineralogy and Petrology* **172**, 7. https://doi.org/10.1007/s00410-016-1325-x.

Holness, M. B., Neufeld, J. A., Gilbert, A. J. & Macdonald, R. (2017b). Orientation of tabular mafic intrusions controls the convective vigour and crystallisation style. *Journal of Petrology* **58**, 2035–2053. https://doi.org/10.1093/petrology/egx081.

Holness, M. B., Tegner, C., Nielsen, T. F. D. & Charlier, B. (2017c). The thickness of the mushy layer on the floor of the Skaergaard magma chamber at apatite saturation. *Journal of Petrology* **58**, 909–932. https://doi.org/10.1093/petrology/egx040.

Huppert, H. E. & Turner, J. S. (1991). Comments on 'On convective style and vigor in sheet-like magma chambers' by Bruce D. Marsh. *Journal of Petrology* **32**, 851–854. https://doi.org/10.1093/petrology/32.4.851.

Iezzi, G., Mollo, S., Torresi, G., Ventura, G., Cavallo, A. & Scarlato, P. (2011). Experimental solidification of an andesitic melt by cooling. *Chemical Geology* **283**, 261–273. https://doi.org/10.1016/j.chemgeo.2011.01.024.

Irvine, T. N. (1970). Heat transfer during solidification of layered intrusions. I. Sheets and sills. *Canadian Journal of Earth Sciences* **7**, 1031–1061. https://doi.org/10.1139/e70-098.

Jarvis, R. A. & Woods, A. W. (1994). The nucleation, growth and settling of crystals from a turbulently convecting fluid. *Journal of Fluid Mechanics* **273**, 83–107. https://doi.org/10.1017/S0022112094001850.

Jaupart, C. & Brandeis, G. (1986). The stagnant bottom layer of convecting magma chambers. *Earth and Planetary Science Letters* **80**, 183–199. https://doi.org/10.1016/0012-821X(86)90032-4.

Jaupart, C. & Tait, S. (1995). Dynamics of differentiation in magma reservoirs. *Journal of Geophysical Research* **100**, 17615–17636. https://doi.org/10.1029/95JB01239.

Kirkpatrick, R. J. (1977). Nucleation and growth of plagioclase, Makaopuhi and Alae lava lakes, Kilauea Volcano. *Hawaii. Geological Society of America Bulletin* **88**, 78–84. https://doi.org/10.1130/0016-7606(1977)88<78:NAGOPM>2.0.CO;2.

Kirkpatrick, R. J., Robinson, G. R. & Hays, J. F. (1976). Kinetics of crystal growth from silicate melts: anorthite and diopside. *Journal of Geophysical Research* **81**, 5715–5720. https://doi.org/10.1029/JB081i032p05715.

Kouchi, A., Tsuchiyama, A. & Sunagawa, I. (1986). Effect of stirring on crystallization kinetics of basalt: texture and element partitioning. *Contributions to Mineralogy and Petrology* **93**, 429–438. https://doi.org/10.1007/BF00371713.

Koyaguchi, T., Hallworth, M. A., Huppert, H. E. & Sparks, R. S. J. (1990). Sedimentation of particles from a convecting fluid. *Nature* **343**, 447–450. https://doi.org/10.1038/343447a0.

Latypov, R. (2014). Reply to 'Comments by Fergus GF Gibb and C. Michael B. Henderson on "M afic–ultramafic sills: new insights from M-and S-shaped mineral and whole-rock compositional profiles"'. *Journal of Petrology* **55**, 1015–1017. https://doi.org/10.1093/petrology/egu014.

Latypov, R. & Chistyakova, S. (2009). Phase equilibria testing of a multiple pulse mechanism for origin of mafic–ultramafic intrusions: a case example of the Shiant Isles Main Sill, NW Scotland. *Geological Magazine* **146**, 851–875. https://doi.org/10.1017/S0016756809006499.

Mangler, M. F., Hunphreys, M. C. S., Wadsworth, F. B., Iveson, A. A. & Higgins, M. D. (2022). Variation of plagioclase shape with size in intermediate magmas: a window into incipient plagioclase crystallisation. *Contributions to Mineralogy and Petrology* **177**, 64. https://doi.org/10.1007/s00410-022-01922-9.

Marsh, B. D. (1988). Crystal capture, sorting, and retention in convecting magma. *Geological Society of America Bulletin* **100**, 1720–1737. https://doi.org/10.1130/0016-7606(1988)100<1720:CCSARI>2.3.CO;2.

Marsh, B. D. (1989). On convective style and vigor in sheet-like magma chambers. *Journal of Petrology* **30**, 479–530. https://doi.org/10.1093/petrology/30.3.479.

Marsh, B. D. (1991). Reply to comments. *Journal of Petrology* **32**, 855–860. https://doi.org/10.1093/petrology/32.4.855.

Marsh, B. D. (1996). Solidification fronts and magmatic evolution. *Mineralogical Magazine* **60**, 5–40. https://doi.org/10.1180/minmag.1996.060.398.03.

Marsh, B. D. & Maxey, M. R. (1985). On the distribution and separation of crystals in convecting magma. *Journal of Volcanology and Geothermal Research* **24**, 95–150. https://doi.org/10.1016/0377-0273(85)90030-7.

Martin, D. & Nokes, R. (1988). Crystal settling in a vigorously converting magma chamber. *Nature* **332**, 534–536. https://doi.org/10.1038/332534a0.

Martin, D. & Nokes, R. (1989). A fluid-dynamical study of crystal settling in convecting magmas. *Journal of Petrology* **30**, 1471–1500. https://doi.org/10.1093/petrology/30.6.1471.

Martin, D., Griffiths, R. W. & Campbell, I. H. (1987). Compositional and thermal convection in magma chambers. *Contributions to Mineralogy and Petrology* **96**, 465–475. https://doi.org/10.1007/BF01166691.

Mathison, C. I. (1987). Pyroxene oikocrysts in troctolitic cumulates–evidence for supercooled crystallization and postcumulus modification. *Contributions to Mineralogy and Petrology* **97**, 228–236. https://doi.org/10.1007/BF00371242.

Meurer, W. P. & Boudreau, A. E. (1998). Compaction of igneous cumulates part II: compaction and the development of igneous foliations. *Journal of Geology* **106**, 293–304. https://doi.org/10.1086/516023.

Mills, R. D., Ratner, J. J. & Glazner, A. F. (2011). Experimental evidence for crystal coarsening and fabric development during temperature cycling. *Geology* **39**, 1139–1142. https://doi.org/10.1130/G32394.1.

Morse, S. A. (1986). Convection in aid of adcumulus growth. *Journal of Petrology* **27**, 1183–1214. https://doi.org/10.1093/petrology/27.5.1183.

Morse, S. A. (2011). The fractional latent heat of crystallising magmas. *American Mineralogist* **96**, 682–689. https://doi.org/10.2138/am.2011.3613.

Muncill, G. E. & Lasaga, A. C. (1987). Crystal-growth kinetics of plagioclase in igneous systems: one-atmosphere experiments and application of a simplified growth model. *American Mineralogist* **72**, 299–311.

Nicoli, G. & Matthews, S. (2019). The Hebridean Igneous Province plumbing system: a phase equilibria perspective. *Lithos* **348-349**, 105194. https://doi.org/10.1016/j.lithos.2019.105194.

Patočka, V., Tosi, N. & Calzavarini, E. (2022). Residence time of inertial particles in 3D thermal convection: implications for magma reservoirs. *Earth and Planetary Science Letters* **591**, 117622. https://doi.org/10.1016/j.epsl.2022.117622.

Philpotts, A. R. & Ague, J. (2009) *Principles of Igneous and Metamorphic Petrology*. Cambridge: Cambridge University Press. https://doi.org/10.1017/CBO9780511813429.

Philpotts, A. R. & Dickson, L. D. (2000). The formation of plagioclase chains during convective transfer in basaltic magma. *Nature* **406**, 59–61. https://doi.org/10.1038/35017542.

Philpotts, A. R. & Philpotts, D. E. (2005). Crystal-mush compaction in the Cohassett flood-basalt flow, Hanford, Washing-

ton. *Journal of Volcanology and Geothermal Research* **145**, 192–206. https://doi.org/10.1016/j.jvolgeores.2005.01.008.

Philpotts, A. R., Shi, J. & Brustman, C. (1998). Role of plagioclase crystal chains in the differentiation of partly cystallised basaltic magma. *Nature* **395**, 343–346. https://doi.org/10.1038/26404.

Philpotts, A. R., Brustman, C. M., Shi, J., Carlson, W. D. & Denison, C. (1999). Plagioclase-chain networks in slowly cooled basaltic magma. *American Mineralogist* **84**, 1819–1829. https://doi.org/10.2138/am-1999-11-1209.

Pupier, E., Duchêne, S. & Toplis, M. J. (2008). Experimental quantification of plagioclase crystal size distribution during cooling of a basaltic liquid. *Contributions to Mineralogy and Petrology* **155**, 555–570. https://doi.org/10.1007/s00410-007-0258-9.

Schiavi, F., Walte, N. & Keppler, H. (2009). First *in situ* observation of crystallization processes in a basaltic-andesitic melt with the moissanite cell. *Geology* **37**, 963–966. https://doi.org/10.1130/G30087A.1.

Schneider, C. A., Rasband, W. S. & Eliceiri, K. W. (2012). NIH Image to ImageJ: 25 years of image analysis. *Nature Methods* **9**, 671–675. https://doi.org/10.1038/nmeth.2089.

Schofield, N. (2009) *Linking sill morphology to emplacement mechanisms*. Unpublished Ph.D. thesis,. University of Birmingham.

Schwindinger, K. R. (1999). Particle dynamics and aggregation of crystals in a magma chamber with application to Kilauea Iki olivines. *Journal of Volcanology and Geothermal Research* **88**, 209–238. https://doi.org/10.1016/S0377-0273(99)00009-8.

Schwindinger, K. R. & Anderson, A. T. (1989). Synneusis of Kilauea Iki olivines. *Contributions to Mineralogy and Petrology* **103**, 187–198. https://doi.org/10.1007/BF00378504.

Sparks, R. S. J. (1990). Crystal capture, sorting, and retention in convecting magma: discussion and reply. *Geological Society of American Bulletin* **102**, 847–850. https://doi.org/10.1130/0016-7606(1990)102<0847:CCSARI>2.3.CO;2.

Stickels, C. A. & Hücke, E. E. (1964). Measurement of dihedral angles. *Transactions of the Metallurgical Society of AIME* **230**, 795–801.

Tait, S. & Jaupart, C. (1989). Compositional convection in viscous melts. *Nature* **338**, 571–574. https://doi.org/10.1038/338571a0.

Tait, S. & Jaupart, C. (1992). Compositional convection in a reactive crystalline mush and melt differentiation. *Journal of Geophysical Research* **97**, 6735–6756. https://doi.org/10.1029/92JB00016.

Turner, J. S. (1979) *Buoyancy Effects in Fluids*. Cambridge: Cambridge University Press.

Walker, F. (1931). VII.—Differentiation in the sills of Northern Trotternish (Skye). *Transactions of the Royal Society of Edinburgh* **57**, 241–257. https://doi.org/10.1017/S0080456800016677.

Wieser, P. E., Vukmanovic, Z., Kilian, R., Ringe, E., Holness, M. B., Maclennan, J. & Edmonds, M. (2019). To sink, swim, twin, or nucleate: a critical appraisal of crystal aggregation processes. *Geology* **47**, 948–952. https://doi.org/10.1130/G46660.1.

Worster, M. G., Huppert, H. E. & Sparks, R. S. J. (1990). Convection and crystallisation in magma cooled from above. *Earth and Planetary Science Letters* **101**, 78–89. https://doi.org/10.1016/0012-821X(90)90126-I.